Can the lack of fibrillar form of alpha-synuclein in Lewy bodies be explained by its catalytic activity?

Ivan A. Kuznetsov[(a), (b)] and Andrey V. Kuznetsov[(c)]

[(a)] Perelman School of Medicine, University of Pennsylvania, Philadelphia, PA 19104, USA

[(b)] Department of Bioengineering, University of Pennsylvania, Philadelphia, PA 19104, USA

[(c)] Department of Mechanical and Aerospace Engineering, North Carolina State University, Raleigh, NC 27695-7910, USA; e-mail: avkuznet@ncsu.edu

Abstract

Finding the causative pathophysiological mechanisms for Parkinson's disease (PD) is important for developing therapeutic interventions. Until recently, it was believed that Lewy bodies (LBs), the hallmark of PD, are mostly composed of alpha-synuclein (α-syn) fibrils. Recent results (Shahmoradian et al., Lewy pathology in Parkinson's disease consists of crowded organelles and lipid membranes, Nature Neuroscience 22 (2019) 1099-1109) demonstrated that the fibrillar form of α-syn is lacking from LBs. Here we propose that this surprising observation can be explained by the catalytic activity of the fibrillar form of α-syn. We assumed that α-syn fibrils catalyze the formation of LBs, but do not become part of them. We developed a mathematical model based on this hypothesis. By using the developed model, we investigated the consequences of this hypothesis. In particular, the model suggests that the long incubation time of PD can be explained by a two-step aggregation process that leads to its development: (i) aggregation of monomeric α-syn into α-syn oligomers and fibrils and (ii) clustering of membrane-bound organelles, which may cause disruption of axonal trafficking and lead to neuron starvation and death. The model shows that decreasing the rate of destruction of α-syn aggregates in somatic lysosomes accelerates the formation of LBs. Another consequence of the model is the prediction that removing α-syn aggregates from the brain after the aggregation of membrane-bound organelles into LBs has started may not stop the progression of PD because LB formation is an autocatalytic process; hence, the formation of LBs will be catalyzed by aggregates of membrane-bound organelles even in the absence of α-syn aggregates. The performed sensitivity study made it possible to establish the hierarchy of model parameters with respect to their effect on the formation of vesicle aggregates in the soma.

Keywords neuron; axon; Parkinson's disease; mathematical modeling; alpha-synuclein

1. Introduction

Parkinson's disease (PD) is a progressive neurodegenerative disorder. No cures or treatments that slow disease progression exist. The only available treatments are dopaminergic drugs [1,2] and deep brain stimulation [3], which only provide symptomatic treatment. PD is caused by the death of dopaminergic (DA) neurons in the brain region called substantia nigra pars compacta (SNc). A post-mortem examination found the presence of abnormal aggregates called Lewy bodies (LBs) (in the soma) and Lewy neurites (LNs) (in the axon) [3].

Until recently it was believed that misfolded fibrillar α-syn is the main component of LBs [4]. Surprisingly, a recent report found that LBs are mostly composed of membrane fragments, organelles, vesicular structures, and various lipid constituencies [5]. The reasons behind these surprising observations are still debated [6]. There is strong evidence suggesting that misfolded and fibrillated α-syn is the pathogen that causes PD [7]. The spread of misfolded α-syn occurs very slowly. It takes ~10 years for Lewy pathology (LBs and LNs) to spread into grafted neuronal cells [8,9]. Understanding whether α-syn aggregates are the PD-causing agents is important because removing the PD-causing agents should lead to remission and stabilization of the disease [10]. Thus, identifying the correct disease-causing agents can have significant impacts on developing effective disease-modifying therapies.

Despite some recent progress in modeling PD [11-13], the urgency for further progress in understanding fundamentals of PD is dictated by the need to develop disease-modifying treatments. Here we develop a model based on the hypothesis that the formation of LBs and LNs is catalyzed by α-syn aggregates (Fig. 1). This would explain why [5] did not find α-syn fibrils in LBs. Our hypothesis would also help to explain another paradox associated with PD: if misfolded α-syn is the disease-causing agent, as it is believed by many researchers [14-17], why does the premotor phase of PD take 20 years or more [3,18]? If transport of misfolded α-syn is the limiting factor, the duration of the premotor phase of the disease should be weeks rather than years [19]. We hypothesize that the long premotor phase of PD can be explained by the requirement for two consecutive aggregation processes: one that leads to the formation of pathological α-syn aggregates and a second that leads to the aggregation of various membrane-bound organelles into LBs. We hypothesize that the second aggregation process requires α-syn aggregates as a catalyst.

2. Methods and models

The model is composed of five submodels detailed in sections 2.1-2.5 and illustrated in Fig. 2. In developing our model, we split all processes into two types: (1) relatively fast processes, which quickly reach steady-state and are simulated using quasi-steady-state equations; (2) extremely slow processes, which take years or decades and eventually lead to the formation of α-syn aggregates and are modeled by transient equations. For example, there is no steady-state for the formation of Lewy bodies, these inclusions slowly grow until a neuron dies, so their formation is an inherently transient process.

2.1. Equations simulating slow axonal transport and diffusion of α-syn monomers from the soma to the synapse (Fig. 2a)

α-syn monomers are synthesized in the soma. However, α-syn monomers have a very small concentration in the soma; they are transported to the axonal arbor, where they accumulate [20]. Transport of α-syn monomers mostly occurs in the slow component-b (SCb) [21-23]. In this paper, we neglect the 10-15% of α-syn monomers that may be transported in fast axonal transport [23]. Slow axonal transport is characterized by fast, short movements that can be either anterograde or retrograde and are probably driven by kinesin and dynein motors [24]. Rapid movements are interrupted by long pauses, during which the α-syn monomers are thought to retain some interaction with MTs.

The sub-model suggested here for transport of α-syn in its monomeric form is based on the model of slow axonal transport of neurofilaments (transported in slow component-a, SCa). This model was developed in [25]. In our previous work, we extended this model to cytosolic proteins, which are transported in SCb and can diffuse in the cytosol [26,27]. For the α-syn monomers, the model contains anterograde and retrograde motor-driven states with concentrations n_a^* and n_r^*, respectively (Fig. 2a). The following equations are obtained by stating the conservation of α-syn in these motor-driven states:

$$-v_a^* \frac{\partial n_a^*}{\partial x^*} - \gamma_{10}^* n_a^* + \gamma_{01}^* n_{a0}^* = 0\,, \tag{1}$$

$$v_r^* \frac{\partial n_r^*}{\partial x^*} - \gamma_{10}^* n_r^* + \gamma_{01}^* n_{r0}^* = 0\,. \tag{2}$$

The first terms on the left-hand sides of Eqs. (1) and (2) describe anterograde (occurring with a velocity v_a^*) and retrograde (occurring with a velocity v_r^*) motions of the α-syn monomers, respectively, while other terms describe transitions between motor-driven and pausing kinetic states. Various kinetic states

and transitions between them are depicted in Fig. 2a; the transitions are characterized by kinetic rates γ^*s. Asterisks denote dimensional quantities.

Equations for the α-syn monomers in two pausing states, with concentrations n^*_{a0} and n^*_{r0}, are also included in the model (Fig. 2a). Despite pausing, it is believed that the α-syn monomers retain some interaction with the MTs and can resume anterograde or retrograde motion. Only the terms that characterize transitions to/from other kinetic states are used in equations expressing conservation of α-syn monomers in the pausing states.

$$-\left(\gamma^*_{01}+\gamma^*_{ar}+\gamma^*_{off,a}\right)n^*_{a0}+\gamma^*_{10}n^*_a+\gamma^*_{ra}n^*_{r0}+\gamma^*_{on,a}n^*_{free}=0\,, \tag{3}$$

$$-\left(\gamma^*_{01}+\gamma^*_{ra}+\gamma^*_{off,r}\right)n^*_{r0}+\gamma^*_{10}n^*_r+\gamma^*_{ar}n^*_{a0}+\gamma^*_{on,r}n^*_{free}=0\,. \tag{4}$$

α-syn monomers in the free (cytosolic) state can be transported by diffusion. Monomeric α-syn can be also degraded in proteasomes [28], which are present in various locations in the axon [29]. It should be noted that α-syn monomers undergoing slow axonal transport in the axon may be protected from significant degradation while in transit, which may result in their longer half-life during axonal transport [30,31]. Cytosolic α-syn monomers can also transition to anterograde or retrograde pausing states. The following equation is obtained by stating the conservation of free monomeric α-syn:

$$D^*_{n_{free}}\frac{\partial^2 n^*_{free}}{\partial x^{*2}}+\gamma^*_{off,a}n^*_{a0}+\gamma^*_{off,r}n^*_{r0}-\left(\gamma^*_{on,a}+\gamma^*_{on,r}\right)n^*_{free}-\frac{n^*_{free}\ln(2)}{T^*_{1/2,\,free}}=0\,. \tag{5}$$

The following boundary conditions are utilized for Eqs. (1)-(5):

At $x^*=0$: $\quad n^*_{tot}=n^*_{tot,x=0}\,,\quad j^*_{tot,\alpha syn\ mon}=v^*_{av,estimate}n^*_{tot,x=0}\,.$ (6a,b)

Eq. (6a) postulates the concentration of free (cytosolic) α-syn monomers at the axon entrance while Eq. (6b) postulates the total flux of newly synthesized α-syn monomers that enter the axon.

The flux of α-syn monomers (positive if anterograde) is found from the following equation:

$$j^*_{tot,\alpha syn\ mon}\left(x^*\right)=-D^*_{n_{free}}\frac{\partial n^*_{free}}{\partial x^*}+v^*_a n^*_a-v^*_r n^*_r\,. \tag{7}$$

The total concentration of α-syn monomers in all five kinetic states displayed in Fig. 2a is found from the following equation:

$$n^*_{tot} = n^*_a + n^*_r + n^*_{a0} + n^*_{r0} + n^*_{free} \,. \tag{8}$$

The following boundary conditions were utilized at the axon presynaptic terminal:

$$\text{At } x^* = L^*: \qquad \frac{\partial n^*_{free}}{\partial x^*} = 0 \,, \qquad n^*_{tot} = n^*_{tot,x=L} \,. \tag{9a,b}$$

Table 1. Independent variables used in the mathematical model of α-syn monomer transport in the axon.

Symbol	Definition	Units
x^*	Cartesian coordinate that originates at the axon hillock and is directed along the axon toward the presynaptic terminal (Fig. 1)	μm
t^*	Time	s

Table 2. Dependent variables used in the mathematical model of α-syn monomer transport in the axon.

Symbol	Definition	Units
$j^*_{tot,\alpha syn\ mon}$	Total flux of α-syn monomers through a given axon cross-section	s^{-1}
n^*_a	Linear number density of on-track α-syn monomers which move along MTs anterogradely, propelled by kinesin molecular motors	μm^{-1}
n^*_r	Linear number density of on-track α-syn monomers which move along MTs retrogradely, propelled by dynein molecular motors	μm^{-1}
n^*_{a0}	Linear number density of pausing on-track α-syn monomers; these monomers are still associated with molecular motors and can resume their anterograde motion	μm^{-1}
n^*_{r0}	Linear number density of pausing on-track α-syn monomers; these monomers are still associated with molecular motors and can resume their retrograde motion	μm^{-1}
n^*_{free}	Linear number density of free (off-track) α-syn monomers in the cytosol, which are not	μm^{-1}

	connected to MTs and can move by diffusion only	

Table 3. Parameters used to characterize the transport of α-syn monomers in the axon. The sensitivity of the area of membrane contained in vesicle aggregates in the soma to these parameters (see section 3.2) is given in the last column. The cells with the largest sensitivity coefficients are shaded grey.

Symbol	Definition	Units	Value or range	Reference(s)	Value(s) used in computations	$S_{\#}^{[D]^*_{s,1,f^*}}$ [a]
$D^*_{n_{free}}$	Diffusivity of α-syn monomers in the free (cytosolic) state	μm²/s	114	[32]	114	-9.14×10^{-7}
L^*	Axon's length	μm	up to 10^6 in humans	[33]	5×10^4 [b]	-1.32×10^{-6}
$n^*_{tot,x=0}$	α-syn monomer concentration at the axon hillock	μM	10^{-3}	[34]	10^{-3}	1.00
$n^*_{tot,x=L}$	α-syn monomer concentration at the presynaptic terminal	μM	3.5	[35]	3.5	-1.45×10^{-6}
$T^*_{1/2,free}$	Half-life of α-syn monomers in the free (cytosolic) state	s	6.62×10^3 - 1.73×10^5	[29,36-38]	5.76×10^{10}	1.59×10^{-5}
v^*_a	Velocities of rapid anterograde motions of α-syn monomers on MTs driven by kinesin motors in slow axonal transport	μm/s	0.7	[39]	0.7	3.34×10^{-5}
v^*_r	Velocities of rapid retrograde motions of α-syn monomers on MTs driven by dynein motors in	μm/s	0.7	[39]	0.7	-3.00×10^{-5}

	slow axonal transport					
$v^*_{av,estimate}$	Estimated average velocity of α-syn monomers in slow axonal transport	μm/s	0.023-0.093 [e]	[30,40,41]	0.05	1.00
γ^*_{10}	Kinetic constant characterizing the rate of transitions $n^*_a \to n^*_{a0}$ and $n^*_r \to n^*_{r0}$ (Fig. 2a)	s^{-1}	7.19×10^{-3}	[42]	7.19×10^{-3}	5.13×10^{-6}
γ^*_{01}	Kinetic constant characterizing the rate of transitions $n^*_{a0} \to n^*_a$ and $n^*_{r0} \to n^*_r$ (Fig. 2a)	s^{-1}	4.01×10^{-3}	[42]	4.01×10^{-3}	4.81×10^{-6}
γ^*_{ar}	Kinetic constant characterizing the rate of transitions $n^*_{a0} \to n^*_{r0}$ (Fig. 2a)	s^{-1}	4.59×10^{-3}	[42]	4.59×10^{-3}	-2.17×10^{-5}
γ^*_{ra}	Kinetic constant characterizing the rate of transitions $n^*_{r0} \to n^*_{a0}$ (Fig. 2a)	s^{-1}	6.76×10^{-3}	[42]	6.76×10^{-3}	1.72×10^{-5}
$\gamma^*_{on,a}$	Kinetic constant characterizing the rate of transitions $n^*_{free} \to n^*_{a0}$ (Fig. 2a)	s^{-1}	9.43×10^{-2}	[42]	9.43×10^{-2}	2.11×10^{-5}
$\gamma^*_{on,r}$	Kinetic constant characterizing the rate of transitions $n^*_{free} \to n^*_{r0}$ (Fig. 2a)	s^{-1}	5.90×10^{-2}	[42]	5.90×10^{-2}	1.48×10^{-6}
$\gamma^*_{off,a}$	Kinetic constant characterizing the rate of transitions	s^{-1}	5.29×10^{-3}	[42]	5.29×10^{-3}	-1.38×10^{-5}

	$n^*_{a0} \rightarrow n^*_{free}$ (Fig. 2a)					
$\gamma^*_{off,r}$	Kinetic constant characterizing the rate of transitions $n^*_{r0} \rightarrow n^*_{free}$ (Fig. 2a)	s^{-1}	5.40×10^{-3}	[42]	5.40×10^{-3}	8.28×10^{-6}

[a] # refers to a corresponding parameter with respect to which the relative sensitivity is calculated, such as $D^*_{c_0}$ (the first row in Table 7), v^*_{-} (the second row in Table 7), etc.

[b] A representative axon length of 50 mm [33] was used.

2.2. Equations simulating transitions between cytoplasmic and membrane-bound α-syn monomers in the presynaptic terminal, clearance of cytoplasmic α-syn monomers in proteasomes, and aggregation of cytoplasmic α-syn monomers (Fig. 2b)

Although α-syn is an intrinsically unstructured protein, it can also interact with membranes [43]. For membrane-bound α-syn, diffusion is restricted to two dimensions, which increases the likelihood of interaction between α-syn monomers and the formation of aggregates [44,45].

In this paper, we simulate aggregation of α-syn monomers (and aggregation of membrane-bound vesicles) using the minimalistic 2-step Finke-Watzky (F-W) model. The first step in the F-W model describes nucleation, $A \rightarrow B$, and is characterized by the rate constant k^*_1. The second step describes aggregate autocatalytic growth, $A+B \rightarrow 2B$, and is characterized by the rate constant k^*_2. k^*_1 and k^*_2 represent effective rates, hiding such processes as fragmentation [46]. In these equations, *A* represents a precursor protein and *B* represents an average of different aggregates of various sizes, including dimers and early oligomers [32,47,48].

We simulate the cytosol of the presynaptic terminal and the presynaptic membrane as two compartments that are in equilibrium. The equation expressing conservation of α-syn monomers (Fig. 1) in the cytosol of the presynaptic terminal is

$$\left(1+\varpi\right)V_{pt}^{*}\frac{d\left[A\right]_{cyt,pt}^{*}}{dt^{*}}=V_{pt}^{*}\left(-k_{1}^{*}\left[A\right]_{cyt,pt}^{*}-k_{2}^{*}\left[A\right]_{cyt,pt}^{*}\left[B\right]_{cyt,pt}^{*}-\frac{\left[A\right]_{cyt,pt}^{*}\ln\left(2\right)}{T_{A,1/2,pt}^{*}}\right)+j_{tot,\alpha syn\ mon}^{*}\left(L^{*}\right)/N_{syn}\,. \tag{10}$$

The equation for the concentration of α-syn monomers in the presynaptic membrane is

$$\left[A\right]_{mem,pt}^{*}=\varpi\frac{V_{pt}^{*}}{A_{pt,mem}^{*}}\left[A\right]_{cyt,pt}^{*}\,. \tag{11}$$

The equation simulating the production of α-syn aggregates (Fig. 1) in the cytosol of the presynaptic terminal is

$$V_{pt}^{*}\frac{d\left[B\right]_{cyt,pt}^{*}}{dt^{*}}=V_{pt}^{*}\left(k_{1}^{*}\left[A\right]_{cyt,pt}^{*}+k_{2}^{*}\left[A\right]_{cyt,pt}^{*}\left[B\right]_{cyt,pt}^{*}\right)+j_{tot,\alpha syn\ aggr}^{*}\left(L\right)/N_{syn}\,, \tag{12}$$

where the flux of α-syn aggregates leaving the presynaptic terminal is

$$j_{tot,\alpha-syn\ aggr}^{*}\left(L^{*}\right)=-D_{c_0}^{*}\frac{\partial c_0^{*}}{\partial x^{*}}-v_{-}^{*}c_{-}^{*}\,. \tag{13}$$

Due to the large number of synapses in DA neuron arbors, in the last terms on the right-hand side of Eqs. (10) and (12) we divided the flux of α-syn monomers coming through the axon to the synapse and the flux of α-syn aggregates transported from the whole arbor to the soma by the number of synapses.

While aggregation of α-syn occurs in the cytosol, nucleation of α-syn aggregates can more likely occur when α-syn is associated with a cellular membrane [45,49]. For that reason, we assumed that the rate constant for the first step of the F-W model for aggregation of α-syn monomers in the cytosol of the presynaptic terminal, k_1^*, is proportional to the area of the active zone of the presynaptic membrane, which is involved in the release of neurotransmitters:

$$k_{1}^{*}=\frac{A_{mem,pt}^{*}}{A_{mem,pt,ref}^{*}}k_{10}^{*}\,, \tag{14}$$

where $A_{mem,pt,ref}^{*}$ is a reference area of the active zone of the presynaptic membrane.

For estimating the volume of the presynaptic terminal, we approximated the terminal as a hemisphere with a diameter D_{pt}^{*}. The area of the presynaptic membrane, which is involved in the release of

neurotransmitters from the presynaptic terminal, is then estimated as that of a circle with the diameter D^*_{pt}:

$$A^*_{mem,pt} = \frac{\pi\left(D^*_{pt}\right)^2}{4}. \tag{15}$$

The flux of the α-syn monomers in the axon is calculated as:

$$j^*_{tot,\alpha-syn\ mon}\left(L^*\right) = -D^*_{n_{free}} \frac{\partial n^*_{free}}{\partial x^*} + v^*_a n^*_a - v^*_r n^*_r \Bigg|_{x^*=L^*}. \tag{16}$$

The following initial conditions are used for Eqs. (10) and (12):

$$\text{At } t^* = 0: \left[A\right]^*_{cyt,pt} = 0,\ \left[B\right]^*_{cyt,pt} = 0. \tag{17}$$

Eq. (17) assumes that initially, the presynaptic terminal does not contain any α-syn monomers, which must be first produced in the soma and then transported to the presynaptic terminal. This is a simplifying assumption because to accurately model the development of α-syn concentration in the presynaptic terminal toward steady-state the growth of the axon needs to be simulated.

Table 4. Dependent variables in the model of α-syn monomers accumulation in the cytosol and membrane of the presynaptic terminal as well as production of α-syn aggregates in the cytosol of the presynaptic terminal.

Symbol	Definition	Units
$\left[A\right]^*_{cyt,pt}$	Volumetric concentration of α-syn monomers in the cytosol of the presynaptic terminal	μm^{-3}
$\left[A\right]^*_{mem,pt}$	Surface concentration of α-syn monomers bound to the presynaptic membrane	μm^{-2}
$\left[B\right]^*_{cyt,pt}$	Volumetric concentration of α-syn aggregates in the cytosol of the presynaptic terminal	μm^{-3}

Table 5. Parameters characterizing accumulation of α-syn monomers in the cytosol and membrane in the presynaptic terminal, as well as production of α-syn aggregates in the cytosol of the presynaptic terminal. The sensitivity of the area of membrane contained in vesicle aggregates in the soma to these parameters

(see section 3.2) is given in the last column. The cells with the largest sensitivity coefficients are shaded grey.

Symbol	Definition	Units	Value or range	Reference(s)	Value(s) used in computations	$S_{\#}^{[D]^*_{s,t_f^*}}$
$A^*_{mem,pt}$	Area of the active zone of the presynaptic membrane, which is involved in the release of neurotransmitters from the presynaptic terminal	μm^2	3.14×10^{-2} - 1.39×10^{-1} [a]	[50,51]	3.14×10^{-2}	9.76×10^{-1}
$A^*_{mem,pt,ref}$	Reference area of the active zone of presynaptic membrane	μm^2			3.14×10^{-2} [b]	-9.75×10^{-1}
k^*_{10}	Rate constant for the first step of the F-W model for aggregation of α-syn monomers in the cytosol of the presynaptic terminal	s^{-1}	2.78×10^{-7} - 9.44×10^{-5}	[32]	3×10^{-7}, 3×10^{-10}	9.76×10^{-1}
$k^*_2 N^*_A$	Rate constant for the second step of the F-W model for aggregation of α-syn monomers in the cytosol of the presynaptic terminal	μm^3 s^{-1} mol^{-1}	1.19×10^{15} - 5.00×10^{15}	[32]	2×10^{15}	1.39×10^{-6} ($S^{[D]^*_{s,t_f^*}}_{k^*_2}$)
N^*_A	Avogadro constant	mol^{-1}	6.022×10^{23}		6.022×10^{23}	
N_{syn}	Number of synapses in a dopamine neuron		2.45×10^5 - 2.4×10^6	[52,53]	2.45×10^5	-2.33×10^{-3}
$T^*_{A,1/2,pt}$	Half-life of α-syn in the monomeric form in the cytosol of the presynaptic terminal	s	6.62×10^3 - 1.73×10^5	[29,36-38]	5.76×10^4	9.72×10^{-1}

V_{pt}^*	Volume of the presynaptic terminal	μm^3	2.09×10^{-3} - 1.94×10^{-2}	[50,51] [a]	2.09×10^{-3}	-2.33×10^{-3}
ϖ	The ratio of the number of α-syn molecules bound to the presynaptic membrane to that in the cytosolic state in the presynaptic terminal		0.1-0.15	[54,55]	0.15	-5.20×10^{-4}

[a] The diameter of the presynaptic terminal is estimated to be between 0.20 μm [50] and 0.42 μm [51].

[b] We used the same value as the area of the presynaptic terminal.

2.3. Equations simulating fast axonal transport of α-syn aggregates inside autophagic vesicles from the presynaptic terminal to the soma (Fig. 2c)

α-syn aggregates are believed to be cleared in lysosomes located in the soma [56]. α-syn aggregates are delivered to lysosomes by autophagy [57]. Autophagosomes move in the fast retrograde component [58], propelled by dynein motors [59,60].

We thus assume that α-syn aggregates are transported retrogradely from the presynaptic terminal to the soma in autophagic vesicles. In the soma, α-syn aggregates are destroyed in lysosomes. Since we consider vesicles that undergo fast axonal transport, in this sub-model we assume that α-syn aggregates can be in two kinetic states: retrograde, when they are transported inside vesicles by retrograde motors, and free, when they are suspended in the cytosol (Fig. 2c). Applying conservation of retrogradely transported α-syn aggregates results in the following equation:

$$v_-^* \frac{\partial c_-^*}{\partial x^*} + \alpha_-^* c_0^* - \alpha_-'^* c_-^* = 0\,, \tag{18}$$

where the first term on the left-hand side describes retrograde motor-driven transport of α-syn aggregates and the last two terms describe the transition of α-syn aggregates to/from the free cytosolic state (Fig. 2c). v_r^* in Eq. (2) and v_-^* in Eq. (18) characterize the retrograde velocities of α-syn monomers and α-syn aggregates, respectively, due to the action of dynein motors. However, these are not velocities of dynein motors per se, but rather effective parameters. This is because modes of axonal transport (slow versus

fast), the average size of the cargo, the average number of motors transporting the cargo, and other parameters that characterize the transport of α-syn monomers and aggregates are different. Therefore, v_r^* and v_-^* may take on different values.

The presence of clusters of fragmented membranous material in LBs [5] suggests that autophagosomes may get damaged during their retrograde transport [61,62], and misfolded α-syn aggregates may escape to the cytosol. Conservation of free α-syn aggregates that are detached from MTs is expressed by the following equation:

$$D_{c_0}^* \frac{\partial^2 c_0^*}{\partial x^{*2}} - \alpha_-^* c_0^* + \alpha_-'^* c_-^* = 0 . \tag{19}$$

Eqs. (18) and (19) are solved subject to the following boundary conditions:

$$\text{At } x^* = 0: \qquad \frac{\partial c_0^*}{\partial x^*} = 0 , \tag{20}$$

where the flux of α-syn aggregates can be found from the following equation:

$$j_{tot,\alpha syn\ aggr}^* = -D_{c_0}^* \frac{\partial c_0^*}{\partial x^*} - v_-^* c_-^* . \tag{21}$$

At the axon presynaptic terminal, we imposed the following boundary conditions:

$$\text{At } x^* = L^*: \qquad c_0^* = A_{pt,b} \left[B\right]_{cyt,pt}^* , \qquad c_-^* = \lambda A_{pt,b} \left[B\right]_{cyt,pt}^* , \tag{22a,b}$$

where

$$A_{pt,b} = \pi \left(D_{pt} / 2 \right)^2 / 4 \tag{23}$$

is the cross-sectional area of the branch connected to the presynaptic terminal. We assumed that the diameter of the branch is half of the diameter of the presynaptic terminal since proteins and vesicles should be able to pass through it.

Eq. (22a) gives the concentration of free (cytosolic) α-syn aggregates in the presynaptic terminal and Eq. (22b) gives the concentration of α-syn aggregates entering the axon from the presynaptic terminal moving retrogradely, which are propelled by dynein motors.

Table 6. Dependent variables in the model of retrograde transport of α-syn aggregates.

Symbol	Definition	Units
c_{-}^{*}	Linear number density of retrogradely transported α-syn aggregates in the axon	μm^{-1}
c_{0}^{*}	Linear number density of free α-syn aggregates in the axon (not actively transported by motors on MTs)	μm^{-1}

Table 7. Parameters characterizing retrograde transport of α-syn aggregates and their estimated values. The sensitivity of the area of membrane contained in vesicle aggregates in the soma to these parameters (see section 3.2) is given in the last column.

Symbol	Definition	Units	Value or range	Reference(s)	Value(s) used in computations	$S_{\#}^{[D]_{s,t_f}^{*}}$
$D_{c_0}^{*}$	Diffusivity of α-syn aggregates in the cytosolic state	μm^2/s	78	[32]	78	7.29×10^{-13}
v_{-}^{*}	Retrograde velocity of α-syn aggregates which are transported in vesicles propelled by dynein motors	μm/s	1.2-1.3	[63]	1.2	2.33×10^{-3}
α_{-}^{*}	Kinetic constant characterizing the rate of transition $c_0^* \rightarrow c_-^*$ (Fig. 2c)	s^{-1}	0.1-1	[64]	1	2.29×10^{-3}
$\alpha_{-}^{\prime *}$	Kinetic constant characterizing the rate of transition $c_-^* \rightarrow c_0^*$ (Fig. 2c)	s^{-1}	0.1-1	[64]	1	-2.29×10^{-3}
λ	Degree of loading of α-syn aggregates that characterizes association of these aggregates with dynein motors at the presynaptic terminal		0.1-10	[64]	1	4.15×10^{-5}

2.4. Equations simulating anterograde fast axonal transport of membrane (via anterograde transport of various membrane-bound vesicles) from the soma to the presynaptic terminal and

catalysis of formation of vesicle aggregates (which eventually form LNs) by aggregated α-syn in the axon (Fig. 2d)

We assume that various membrane-bound vesicles synthesized in the soma are transported toward the presynaptic terminal anterogradely by fast axonal transport. This leads to the flow of the membrane from the soma toward the synapse. Since vesicles are transported by kinesin motors pulling them along MTs, one of the kinetic states in the model represents anterogradely moving vesicles. It is also assumed that vesicles can detach from MTs and become freely suspended in the cytosol (Fig. 2d). Applying conservation of anterogradely transported membrane gives the following equation:

$$-v_{+}^{*}\frac{\partial b_{+}^{*}}{\partial x^{*}}+\beta_{+}^{*}b_{0}^{*}-\beta_{+}^{\prime *}b_{+}^{*}=0\,, \tag{24}$$

where the first term on the left-hand side describes anterograde motor-driven vesicle transport and the last two terms describe transitions between anterograde motor-driven state and free (cytosolic) state (Fig. 2d). v_{a}^{*} and v_{+}^{*} characterize the anterograde velocities of α-syn monomers and anterogradely transported vesicles, respectively, due to the action of kinesin motors. These, however, are not kinesin motor velocities as such, but rather effective parameters. This is due to the differences in axonal transport modes (slow versus fast), cargo average size, the average number of motors interacting with cargo, and other parameters distinguishing α-syn and vesicles transport. As a result, values of v_{a}^{*} and v_{+}^{*} may be different.

Conservation of membrane in the vesicles that are detached from MTs and freely suspended in the cytosol is expressed by the following equation:

$$-\beta_{+}^{*}b_{0}^{*}+\beta_{+}^{\prime *}b_{+}^{*}-k_{3,ax}^{*}b_{0}^{*}-k_{4,ax}^{*}b_{0}^{*}b_{aggr,ax}^{*}=0\,. \tag{25}$$

The first two terms in Eq. (25) are kinetic terms describing transitions between anterogradely running and free kinetic states of vesicles (Fig. 2c). The last two terms in Eq. (25) describe the decrease in the concentration of free vesicles in the cytosol due to the production of vesicle aggregates. Simulation of this process is important for understanding the formation of LBs, which involves the sequestration of proteins, organelles, lipids, and endomembranes and their packing and compaction into LB-like inclusions [5,65,66]. These last two terms in Eq. (25) are written utilizing the F-W model. The mechanism of vesicle aggregates formation combines primary nucleation (described by the kinetic constant $k_{3,ax}^{*}$ in Eq. (25)) and secondary nucleation (described by the kinetic constant $k_{4,ax}^{*}$). Accumulation of membrane contained in vesicle aggregates is described by the following equation:

$$\frac{\partial b^*_{aggr,ax}}{\partial t^*} = k^*_{3,ax} b^*_0 + k^*_{4,ax} b^*_0 b^*_{aggr,ax} , \quad (26)$$

where the diffusivity of vesicle aggregates was neglected because of their large size.

We assumed that the nucleation step in the formation of vesicle aggregates is catalyzed by α-syn aggregates, for which reason α-syn aggregates do not become a part of LBs. It was observed that α-syn fibrils can "absorb" lipid vesicles causing their clustering [67]. Therefore, it is possible that while misfolded α-syn aggregates are delivered to the soma for degradation, they catalyze clustering of various membrane-bound vesicles in the axon. Thus, we assume that the rate of formation of vesicle aggregates in the axon is proportional to the concentration of free (suspended in the cytosol) α-syn aggregates in the axon:

$$k^*_{3,ax} = c^*_0 k^*_{30,ax} . \quad (27)$$

Eqs. (24) and (25) must be solved subject to the following boundary conditions:

$$\text{At } x^* = 0: \qquad j^*_{tot,mem} = j^*_{tot,mem,x=0} , \quad (28)$$

where

$$j^*_{tot,mem}\left(x^*\right) = v^*_+ b^*_+\left(x^*\right) \quad (29)$$

and $j^*_{tot,mem,x=0}$ is the rate at which membrane contained in membrane-bound vesicles enters the axon from the soma (the rate of synthesis of the membrane contained in the axonal cargo in the soma).

Eq. (26) must be solved subject to the following initial condition:

$$\text{At } t^* = 0: \qquad b^*_{aggr,ax} = 0 . \quad (30)$$

Table 8. Dependent variables in the model of anterograde transport of membrane in synaptic vesicles and its aggregation in the axon.

Symbol	Definition	Units
b^*_+	Total area of membrane in all membrane-bound organelles that are actively anterogradely transported in the axon, per unit length of the axon	$\mu m^2\ \mu m^{-1}$

b_0^*	Total area of membrane in all membrane-bound organelles that are detached from MTs (not actively transported), per unit length of the axon	$\mu m^2\ \mu m^{-1}$
$b_{aggr,ax}^*$	Total area of membrane in all vesicle aggregates in the axon (that later become LNs), per unit length of the axon	$\mu m^2\ \mu m^{-1}$

Table 9. Parameters characterizing anterograde vesicle transport and aggregation in the axon. The sensitivity of the area of membrane contained in vesicle aggregates in the soma to these parameters (see section 3.2) is given in the last column.

Symbol	Definition	Units	Value or range	Reference(s)	Value(s) used in computations	$S_{\#}^{[D]^*_{s,t_f^*}}$
$j_{tot,mem,x=0}^*$	Membrane flux, via transport of membrane-bound organelles, in an axon (the rate of synthesis of the membrane in the soma)	$\mu m^2\ s^{-1}$	0.833	[68]	0.833	0.00
v_+^*	Average velocity of anterogradely transported membrane-bound organelles propelled by kinesin motors	μm/s	0.9	[68]	0.9	0.00
β_+^*	Kinetic constant characterizing the rate of transition $b_0^* \rightarrow b_+^*$ (Fig. 2d)	s^{-1}	0.1-10	[64]	1	0.00
$\beta_+'^*$	Kinetic constant characterizing the rate of transition $b_+^* \rightarrow b_0^*$ (Fig. 2d)	s^{-1}	0.1-10	[64]	1	0.00
$k_{30,ax}^*$	Proportionality constant determining the first step of the F-W model for vesicle aggregation in the axon	$\mu m\ s^{-1}$	2.78×10^{-7} - 9.44×10^{-5}	[32]	10^{-5}	0.00

$\frac{k^*_{4,ax}N^*_A}{3A_{ax,1}A_{c,ax}}$ [a]	Rate constant for the second step of the F-W model for vesicle aggregation in the axon	μm^{-1} s^{-1} mol^{-1}	1.19×10^{15} - 5.00×10^{15}	[32]	3×10^{15}	0.00 ($S^{[D]^*_{s,1f}}_{k^*_{4,ax}}$)

[a] For this estimate, as a characteristic area of the internal membrane, we used the area of the internal membrane inside a segment of the axon with a length of 1 μm. The area of the internal membrane is assumed to be three times larger than the area of the plasma membrane around that segment of the axon, $A^*_{ax,1} = \pi D^*_{ax}(1\ \mu m)$. Also, $A^*_{c,ax} = \pi D^{*2}_{ax}/4$, where D^*_{ax} is the diameter of the axon, which is estimated to be 0.7 μm [69].

2.5. Equations describing the destruction of α-syn aggregates in the somatic lysosomes and catalysis of the formation of vesicle aggregates (which ultimately leads to the formation of LBs) by α-syn aggregates in the soma (Fig. 2e)

It is likely that under normal conditions α-syn monomers are destroyed in proteasomes while α-syn aggregates are destroyed in lysosomes [28]. We thus assumed that α-syn monomers are degraded in proteasomes, which are present in various locations in the axon, while α-syn aggregates are degraded in lysosomes, which are mostly located in the soma [70].

The process of destruction of α-syn aggregates in the lysosomes in the soma is modeled by the following equation:

$$\frac{d[B]^*_{cyt,s}}{dt} = -j^*_{tot,\alpha-syn\ aggr}(0)/V^*_s - \frac{[B]^*_{cyt,s}\ln(2)}{T^*_{B,1/2,s}}, \tag{31}$$

where

$$j^*_{tot,\alpha-syn\ aggr}(0) = -D^*_{c_0}\frac{\partial c^*_0}{\partial x^*} - v^*_- c^*_-. \tag{32}$$

The negative sign before the first term of the right-hand side of Eq. (31) is because α-syn aggregates enter the soma by retrograde transport from the axon.

We assumed that α-syn aggregates catalyze the formation of vesicle aggregates in the soma. We used the F-W model to simulate the formation of vesicle aggregates:

$$\frac{d[D]_s^*}{dt} = k_{3,s}^* [C]_{s0}^* + k_{4,s}^* [C]_{s0}^* [D]_s^* . \quad (33)$$

Similar to Eq. (27), we assumed that the nucleation step in the formation of vesicle aggregates is catalyzed by α-syn aggregates, and thus the rate of formation of vesicle aggregates in the soma is proportional to the concentration of α-syn aggregates in the soma:

$$k_{3,s}^* = [B]_{cyt,s}^* k_{30,s}^* . \quad (34)$$

Eqs. (31), (33), and (34) must be solved subject to the following initial conditions:

$$\text{At } t^* = 0: \qquad [B]_{cyt,s}^* = 0 , \qquad [D]_s^* = 0 . \quad (35)$$

Table 10. Dependent variables in the model describing the formation of vesicle aggregates and α-syn aggregates destruction in the soma.

Symbol	Definition	Units
$[B]_{cyt,s}^*$	Volumetric concentration of α-syn aggregates in the cytosol of the soma	μm^{-3}
$[D]_s^*$	Volumetric concentration of membrane in membrane fragments and fragmented organelles that were found in LBs in [5]	$\mu m^2 \mu m^{-3}$

Table 11. Parameters characterizing the formation of vesicle aggregates and α-syn aggregates destruction in the soma. The sensitivity of the area of membrane contained in vesicle aggregates in the soma to these parameters (see section 3.2) is given in the last column. The cells with the largest sensitivity coefficients are shaded grey.

Symbol	Definition	Units	Value or range	Reference(s)	Value(s) used in computations	$S_{\#}^{[D]_{s,t_f^*}^*}$
$[C]_{s0}^*$	Volumetric concentration of membrane in the membrane-bound vesicles in the soma	$\mu m^2 \mu m^{-3}$	0.9 [a]		0.9	4.27

$k^*_{30,s}$	Proportionality constant determining the first step of the F-W model for vesicle aggregation in the soma	μm s^{-1}	2.78×10^{-7} - 9.44×10^{-5}	[32]	10^{-5}	1.00
$\frac{k^*_{4,s}N^*_A}{3A_{s,1}}$ [b]	Rate constant for the second step of the F-W model for vesicle aggregation in the soma	μm s^{-1} mol^{-1}	1.19×10^{15} - 5.00×10^{15}	[32]	3×10^{15}	3.27 ($S^{[D]^*_{s,tf}}_{k^*_{4,s}}$)
$T^*_{B,1/2,s}$	Average half-life of α-syn aggregates before their destruction in somatic lysosomes	s	5.76×10^{4} - 7.78×10^{5}	[71]	2.59×10^{5}	9.84×10^{-1}
V^*_s	Volume of the soma	μm^3	4.189×10^{3} [c]	[72]	4.189×10^{3}	−1.00

[a] We assumed that the area of the internal membrane inside the soma is three times larger than the area of the plasma membrane.

[b] For the characteristic area of plasma membrane we used $A_{s,1} = \pi(1\ \mu m)^2$, which is the area of plasma membrane around a sphere with a diameter of 1 μm.

[c] Based on a representative soma diameter, D^*_s, of 20 μm.

3. Results

The model predicts that most α-syn monomers localize in the presynaptic terminal, which is consistent with [43,73] (Fig. 3a). The flux of α-syn monomers in the axon remains constant because we assumed that α-syn monomers are protected from degradation during their transport in the axon, and hence under steady-state conditions, their flux must be independent of the position in the axon (Fig. 3b).

α-syn monomers exist in the cytosol of the presynaptic terminal in equilibrium with membrane-bound α-syn monomers [43]. Both volumetric and surface concentrations quickly reach their steady-state values (Fig. 4a). The concentration of α-syn aggregates in the cytosol also quickly reaches its steady-state value (Fig. 4b). This equilibrium value is controlled by the rate of production of aggregates in the presynaptic terminal and their removal into the axon by retrograde transport to the soma for degradation in lysosomes.

Linear number densities of retrogradely transported α-syn aggregates and free α-syn aggregates in the axon are uniform (Fig. 5). They take on the same values due to the choice of values of kinetic constants, α_{-}^{*} and $\alpha_{-}^{\prime *}$ (Table 7).

The total area of membrane contained in all membrane-bound organelles traveling anterogradely in the axon and suspended in the axon's cytoplasm is uniform along the axon (Fig. 6). The flux of anterogradely transported vesicles in the axon is also uniform due to a small rate of vesicle aggregation (small values of $k_{3,ax}^{*}$ and $k_{4,ax}^{*}$, Table 9 and Eq. (27)).

The total area of the membrane in all vesicle aggregates in the axon is uniformly distributed along the length of the axon (Fig. 7a). The total area of the membrane in all vesicle aggregates in the middle of the axon monotonically (but not linearly) increases with time, with the rate of the increase becoming larger over time, which follows from the curvature of the line in Fig. 7b.

Failure of clearance of α-syn aggregates in lysosomes may result in the accumulation of toxic oligomeric species of α-syn in the soma [74-76]. Interestingly, the excessive amount of aggregated α-syn can lead to the impairment of lysosomal activity, and hence cause a vicious cycle of even more accumulation of misfolded α-syn in the soma [77]. To test the effects of a longer half-life of α-syn aggregates in the soma we performed computations with two values of the half-life of α-syn aggregates in the soma: 2.59×10^{5} and 2.59×10^{10} s. The volumetric concentration of α-syn aggregates in the soma increases much faster for the larger half-life of α-syn aggregates (Fig. 8a). Since we assumed that α-syn aggregates catalyze clustering of membrane-bound vesicles in the soma (Eq. (34)), the amount of membrane contained in vesicle clusters also increases much faster for a large half-life of α-syn aggregates (Fig. 8b). Other quantities in the model are not affected (data not shown).

It is important to understand whether the progress of PD can be stopped by removing the α-syn aggregates. The removal can potentially be accomplished by boosting autophagic/lysosomal clearance as well as using intra/nanobodies for immunotherapy [78]. Another approach is using oligomer modulators, such as Anle138b, to inhibit the formation and accumulation of α-syn oligomers [79]. To simulate this situation, we removed all α-syn aggregates from the system 1 year after the formation of LBs started (dotted line in Fig. 8a). Surprisingly, the accumulation of vesicle aggregates continued, although at a slower pace (dotted line in Fig. 8b). This is explained as follows. Even if the nucleation of vesicle aggregates is suddenly stopped, the autocatalytic formation of vesicle aggregates continues. This is because in the F-W model there are two mechanisms of aggregate growth: nucleation and autocatalytic growth. This means that although PD could be initialed by α-syn oligomers, the removal of these

oligomers from the brain after the formation of LBs has started may not stop the PD progression. This result is consistent with the failure of Phase III trials of Aβ-targeting drugs for Alzheimer's disease (AD). Since the Aβ deposition may begin two decades or even more before clinical symptoms of AD, the administered AD treatment in these trials may simply be too late to stop the disease [80,81].

3.2. Investigating sensitivity of the area of membrane contained in vesicle aggregates in the soma to model parameters

We investigated how the area of the membrane contained in vesicle aggregates by the end of the simulation ($t_f^* = 3.17$ years) depends on model parameters. The analysis was performed by computing the local sensitivity coefficients, which are first-order partial derivatives of the membrane area with respect to the parameters [82-85]. The sensitivity coefficient of $\left[D\right]_{s,t_f^*}^*$ to parameter $n_{tot,x=0}^*$, for example, was calculated as follows:

$$\frac{\partial\left[D\right]_{s,t_f^*}^*}{\partial n_{tot,x=0}^*} \approx \left.\frac{\left[D\right]_{s,t_f^*}^*\left(n_{tot,x=0}^* + \Delta n_{tot,x=0}^*\right) - \left[D\right]_{s,t_f^*}^*\left(n_{tot,x=0}^*\right)}{\Delta n_{tot,x=0}^*}\right|_{\text{other parmeters kept constant}}, \tag{36}$$

where $\Delta n_{tot,x=0}^* = 10^{-3} n_{tot,x=0}^*$. The independence of $n_{tot,x=0}^*$ of the step size was tested by using various step sizes.

We then calculated non-dimensionalized relative sensitivity coefficients following [83,86] as (for example):

$$S_{n_{tot,x=0}^*}^{\left[D\right]_{s,t_f^*}^*} = \frac{n_{tot,x=0}^*}{\left[D\right]_{s,t_f^*}^*}\frac{\partial\left[D\right]_{s,t_f^*}^*}{\partial n_{tot,x=0}^*}. \tag{37}$$

The relative sensitivity coefficients are reported in Tables 3, 5, 7, 9, and 11. The concentration of vesicle aggregates in the soma is highly sensitive to the following parameters: $n_{tot,x=0}^*$, $v_{av,estimate}^*$, $A_{mem,pt}^*$, $A_{mem,pt,ref}^*$, k_{10}^*, $T_{A,1/2,pt}^*$, $\left[C\right]_{s0}^*$, $k_{30,s}^*$, $k_{4,s}^*$, $T_{B,1/2,s}^*$, and V_s^* (the range of the absolute value of relative sensitivity is 0.97-4.3). Among those, $\left[C\right]_{s0}^*$, which is the volumetric concentration of membrane in the membrane-bound vesicles in the soma, and $k_{4,s}^*$, which is the rate constant for the second step of the F-W model for vesicle aggregation in the soma, produce the highest relative sensitivity. The concentration of vesicle

aggregates in the soma exhibits medium sensitivity to the following parameters: N_{syn}, V_{pt}^*, ϖ, v_-^*, α_-^*, and $\alpha_-'^*$ (the range of the absolute value of relative sensitivity is 5.2×10^{-4} - 2.4×10^{-3}). The concentration of vesicle aggregates in the soma exhibits low sensitivity to the following parameters: $D_{n_{free}}^*$, L^*, $n_{tot,x=L}^*$, $T_{1/2,free}^*$, v_a^*, v_r^*, γ_{10}^*, γ_{01}^*, γ_{ar}^*, γ_{ra}^*, $\gamma_{on,a}^*$, $\gamma_{on,r}^*$, $\gamma_{off,a}^*$, $\gamma_{off,r}^*$, k_2^*, $D_{c_0}^*$, and λ (the range of the absolute value of relative sensitivity is 7.2×10^{-13} - 4.2×10^{-5}). Finally, parameters given in Table 9 ($j_{tot,mem,x=0}^*$, v_+^*, β_+^*, $\beta_+'^*$, $k_{30,ax}^*$, and $k_{4,ax}^*$) do not affect vesicle aggregates in the soma (the relative sensitivity is 0) because these parameters affect only the events occurring downstream of vesicle aggregation in the soma. However, the parameters that are given in Table 9 affect vesicle aggregation in the axon, as shown in Table S1 in the Supplemental Materials.

If misfolded α-syn is the disease-causing agent, why does the premotor phase of PD span many years [3], [18] while transport of misfolded α-syn aggregates from the synapse to the soma take days or weeks at most [19]? To answer this question, we compared the results presented in Fig. 8 with the results computed for a three orders of magnitude smaller rate constant for the first step of the F-W model for aggregation of α-syn monomers in the presynaptic terminal, $k_{10}^* = 3\times10^{-10}$. The reduction of the α-syn aggregation rate leads to a significant reduction of the concentration of α-syn in the soma (Fig. 9a) as well as to a significant reduction of the concentration of aggregates of membrane-bound vesicles in the soma (Fig. 9b), which are the main component of LBs. The slow rate of PD progression can then be explained by the need to produce α-syn aggregates first, which then catalyze the development of LBs. The formation of α-syn oligomers alone is insufficient for the development of PD, and just initiates the process, which takes much longer than the time required for the production and transport of α-syn aggregates.

4. Discussion, limitations of the model, and future directions

The purpose of this paper was to develop a minimal model for studying the possible effects of aggregated forms of α-syn on LB formation. We propose that such α-syn oligomers and fibrils work as catalysts, facilitating the formation of LBs and LNs, but not becoming a part of them.

The model simulates the transport of α-syn in the axon, production of α-syn aggregates in the synapse due to α-syn interaction with the synaptic membrane, transport of aggregates to the soma for degradation in somatic lysosomes, and catalysis of clustering of membrane-bound vesicles in the soma and the axon by α-syn aggregates.

There is still debate on whether endogenous α-syn oligomers are harmless but can convert to toxic oligomers or all α-syn oligomers are toxic [87]. The model predicts that the formation of a small amount of α-syn aggregates in the presynaptic terminal because of the folding of α-syn monomers due to their interaction with the plasma membrane is a normal process. This model prediction is in agreement with [18] that reported that misfolded α-syn is abundant in presynaptic terminals. The aggregates produced in the terminal are then transported to the soma for degradation in the lysosomes. However, on their way to lysosomes aggregates can catalyze clustering of membrane-bound vesicles. This can happen both in the axon and in the soma, at any time until α-syn aggregates reach lysosomes.

Interestingly, the model predicts that α-syn monomers, transported by slow axonal transport, move against their concentration gradient, with the lowest concentration at the soma and the highest concentration at the presynaptic terminal. The distribution of α-syn monomers along the axon length is, in principle, experimentally measurable and our predictions about α-syn distribution, displayed in Fig. 3a, can be tested in future experiments. Studies of α-syn distribution have been reported, such as [88]. Notably, such studies tend to focus on the distribution of α-syn aggregates because, due to their density, they are much more obvious under light or electron microscopy. However, one can envision an experiment wherein labeling (fluorescence or otherwise) of endogenous α-syn is used to uncover the underlying monomer distribution.

According to model, α-syn aggregates and membrane-bound vesicles, moved by fast axonal transport, exhibit a uniform concentration along the axon. Modeling results confirm that failure of clearance of oligomeric species of α-syn in somatic lysosomes (which was simulated by increasing the half-life of α-syn aggregates in the soma) may lead to the formation of LBs in the soma. According to our hypothesis, this occurs due to more catalytic activity of α-syn aggregates, which leads to the formation of vesicle aggregates in the soma. These aggregates later develop into LBs. This result is in agreement with a mouse model of PD, which shows that low levels of lysosomes precede accumulation of autophagosomes and thus suggests the importance of this clearance pathway in PD [56]. Notably, a recently published set of reporters of α-syn conformation [89] have utility for experimentally validating this phenomenon. These α-syn reporters are based upon fluorescence resonance energy transfer (FRET); changes in α-syn conformation are transduced as changes in FRET efficiency. Therefore, in principle, these reporters allow one to study, at the subcellular level and with high temporal resolution, the progression of α-syn aggregation. Hence, these reporters are broadly useful, not just for validating the previously described hypothesis, but for experimentally confirming many of the other modeling derived hypotheses described here.

Since the formation of LBs is an autocatalytic process, and old vesicle aggregates can catalyze the formation of new vesicle aggregates even in the absence of α-syn aggregates, the model predicts that removing α-syn aggregates after the formation of LBs has begun may not stop the PD progression. Thus after a certain point, the process of LB formation can become self-sustaining. This prediction is both testable and falsifiable. This may have significant implications on PD treatment strategies, as if this prediction is true we should expect to see a broad failure of PD clinical trials focused on therapeutics which reduce the burden of α-syn aggregates after PD is already clinically diagnosed. Indeed, if true, this is suggestive that it is critical to begin treatment of PD early, before classical clinical signs are apparent, and hence necessitating better technologies for early detection of PD.

Future versions of the model should take into account the following. (i) Effect of a complex structure of axonal arbor. DA neurons in SNc have hundreds of thousands of synapses, which is two orders of magnitude more than other neurons in basal ganglia [52], [53], [90]. (ii) Simulating the possible effect of traffic jams caused by aggregation of membrane-bound vesicles. This is important because synaptic degeneration in PD may be caused by the lack of presynaptic proteins, called "vacant synapses" [91]. (iii) Simulating the effect of the 10-15% of α-syn monomers that may be transported in fast axonal transport [23]. (iv) A more precise model of α-syn aggregation in the presynaptic terminal is needed, which should include different pools of α-syn: unbound, soluble monomers, monomers bound to presynaptic vesicles, and microaggregates [92]. An α-syn polymerization model capable of distinguishing between different intermediate forms of α-syn aggregates is needed as well. This is especially important because α-syn oligomers are potentially the true disease-causing species, while large α-syn aggregates such as LBs may be neuroprotective [19], [49], [93]. Future research should use a combination of modeling and experimentation to answer the above-mentioned questions.

Acknowledgment

IAK acknowledges the fellowship support of the Paul and Daisy Soros Fellowship for New Americans and the NIH/National Institutes of Mental Health (NIMH) Ruth L. Kirchstein NRSA (F30 MH122076-01). AVK acknowledges the support of the National Science Foundation (award CBET-2042834) and the Alexander von Humboldt Foundation through the Humboldt Research Award.

References

[1] J. Jankovic, Parkinson's disease: Clinical features and diagnosis, Journal of Neurology Neurosurgery and Psychiatry 79 (2008) 368-376.

[2] D. Charvin, R. Medori, R.A. Hauser, O. Rascol, Therapeutic strategies for Parkinson disease: Beyond dopaminergic drugs, Nature Reviews Drug Discovery 17 (2018) 804-822.

[3] L.V. Kalia, A.E. Lang, Parkinson's disease, Lancet 386 (2015) 896-912.

[4] M.B. Fares, S. Jagannath, H.A. Lashuel, Reverse engineering Lewy bodies: How far have we come and how far can we go? Nature Reviews Neuroscience 22 (2021) 111-131.

[5] S.H. Shahmoradian, A.J. Lewis, C. Genoud, J. Hench, T.E. Moors, P.P. Navarro, D. Castano-Diez, G. Schweighauser, A. Graff-Meyer, K.N. Godie, R. Sutterlin, E. Huisman, A. Ingrassia, Y. de Gier, A.J.M. Rozemuller, J. Wang, A. De Paepe, J. Erny, A. Staempfli, J. Hoernschemeyer, F. Grosserueschkamp, D. Niedieker, S.F. El-Mashtoly, M. Quadri, W.F.J. Van IJcken, V. Bonifati, K. Gerwert, B. Bohrmann, S. Frank, M. Britschgi, H. Stahlberg, W.D.J. Van de Berg, M.E. Lauer, Lewy pathology in Parkinson's disease consists of crowded organelles and lipid membranes, Nature Neuroscience 22 (2019) 1099-1109.

[6] H.A. Lashuel, Do Lewy bodies contain alpha-synuclein fibrils? And does it matter? A brief history and critical analysis of recent reports, Neurobiology of Disease 141 (2020) 104876.

[7] K.C. Luk, V. Kehm, J. Carroll, B. Zhang, P. O'Brien, J.Q. Trojanowski, V.M.-. Lee, Pathological alpha-synuclein transmission initiates Parkinson-like neurodegeneration in nontransgenic mice, Science 338 (2012) 949-953.

[8] J.H. Kordower, Y. Chu, R.A. Hauser, T.B. Freeman, C.W. Olanow, Lewy body-like pathology in long-term embryonic nigral transplants in Parkinson's disease, Nature Medicine 14 (2008) 504-506.

[9] J. Li, E. Englund, J.L. Holton, D. Soulet, P. Hagell, A.J. Lees, T. Lashley, N.P. Quinn, S. Rehncrona, A. Bjorklund, H. Widner, T. Revesz, O. Lindvall, P. Brundin, Lewy bodies in grafted neurons in subjects with Parkinson's disease suggest host-to-graft disease propagation, Nature Medicine 14 (2008) 501-503.

[10] B.H.M. Hunn, S.J. Cragg, J.P. Bolam, M. Spillantini, R. Wade-Martins, Impaired intracellular trafficking defines early Parkinson's disease, Trends in Neurosciences 38 (2015) 178-188.

[11] I.A. Kuznetsov, A.V. Kuznetsov, Mathematical models of alpha-synuclein transport in axons, Computer Methods in Biomechanics and Biomedical Engineering 19 (2016) 515-526.

[12] I.A. Kuznetsov, A.V. Kuznetsov, What can trigger the onset of Parkinson's disease - A modeling study based on a compartmental model of alpha-synuclein transport and aggregation in neurons, Mathematical Biosciences 278 (2016) 22-29.

[13] S. Bakshi, V. Chelliah, C. Chen, P.H. van der Graaf, Mathematical biology models of Parkinson's disease, CPT: Pharmacometrics & Systems Pharmacology 8 (2019) 77-86.

[14] E. Vasili, A. Dominguez-Meijide, T.F. Outeiro, Spreading of alpha-synuclein and tau: A systematic comparison of the mechanisms involved, Frontiers in Molecular Neuroscience 12 (2019) 107.
[15] C. Duyckaerts, F. Clavaguera, M. Potier, The prion-like propagation hypothesis in Alzheimer's and Parkinson's disease, Current Opinion in Neurology 32 (2019) 266-271.
[16] R.K. Leak, M.P. Frosch, T.G. Beach, G.M. Halliday, Alpha-synuclein: Prion or prion-like? Acta Neuropathologica 138 (2019) 509-514.
[17] C. Terry, J.D.F. Wadsworth, Recent advances in understanding mammalian prion structure: A mini review, Frontiers in Molecular Neuroscience 12 (2019) 169.
[18] J.C. Bridi, F. Hirth, Mechanisms of alpha-synuclein induced synaptopathy in Parkinson's disease, Frontiers in Neuroscience 12 (2018) 80.
[19] J.T. Lamberts, E.N. Hildebrandt, P. Brundin, Spreading of alpha-synuclein in the face of axonal transport deficits in Parkinson's disease: A speculative synthesis, Neurobiology of Disease 77 (2015) 276-283.
[20] J.Y. Li, P.H. Jensen, A. Dahlstrom, Differential localization of alpha-, beta- and gamma-synucleins in the rat CNS, Neuroscience 113 (2002) 463-478.
[21] P. Jensen, M. Nielsen, R. Jakes, G. Dotti, M. Goedert, Binding of alpha-synuclein to brain vesicles is abolished by familial Parkinson's disease mutation, Journal of Biological Chemistry 273 (1998) 26292-26294.
[22] P. Jensen, J. Li, A. Dahlstrom, C. Dotti, Axonal transport of synucleins is mediated by all rate components, European Journal of Neuroscience 11 (1999) 3369-3376.
[23] Y. Tang, U. Das, D.A. Scott, S. Roy, The slow axonal transport of alpha-synuclein-mechanistic commonalities amongst diverse cytosolic cargoes, Cytoskeleton 69 (2012) 506-513.
[24] M. Utton, W. Noble, J. Hill, B. Anderton, D. Hanger, Molecular motors implicated in the axonal transport of tau and alpha-synuclein, Journal of Cell Science 118 (2005) 4645-4654.
[25] P. Jung, A. Brown, Modeling the slowing of neurofilament transport along the mouse sciatic nerve, Physical Biology 6 (2009) 046002.
[26] A.V. Kuznetsov, A.A. Avramenko, D.G. Blinov, Effect of protein degradation in the axon on the speed of the bell-shaped concentration wave in slow axonal transport, International Communications in Heat and Mass Transfer 36 (2009) 641-645.
[27] A.V. Kuznetsov, A.A. Avramenko, D.G. Blinov, Macroscopic modeling of slow axonal transport of rapidly diffusible soluble proteins, International Communications in Heat and Mass Transfer 36 (2009) 293-296.

[28] A. Raichur, S. Vali, F. Gorin, Dynamic modeling of alpha-synuclein aggregation for the sporadic and genetic forms of Parkinson's disease, Neuroscience 142 (2006) 859-870.
[29] M.C. Bennett, J.F. Bishop, Y. Leng, P.B. Chock, T.N. Chase, M.M. Mouradian, Degradation of alpha-synuclein by proteasome, Journal of Biological Chemistry 274 (1999) 33855-33858.
[30] W.X. Li, P.N. Hoffman, W. Stirling, D.L. Price, M.K. Lee, Axonal transport of human alpha-synuclein slows with aging but is not affected by familial Parkinson's disease-linked mutations, Journal of Neurochemistry 88 (2004) 401-410.
[31] T. Rosenberg, S. Gal-Ben-Ari, D.C. Dieterich, M.R. Kreutz, N.E. Ziv, E.D. Gundelfinger, K. Rosenblum, The roles of protein expression in synaptic plasticity and memory consolidation, Frontiers in Molecular Neuroscience 7 (2014) 86.
[32] S. Nath, J. Meuvis, J. Hendrix, S.A. Carl, Y. Engelborghs, Early aggregation steps in alpha-synuclein as measured by FCS and FRET: Evidence for a contagious conformational change, Biophysical Journal 98 (2010) 1302-1311.
[33] S. Roy, Finding order in slow axonal transport, Current Opinion in Neurobiology 63 (2020) 87-94.
[34] S.M.L. Banks, A.T. Medeiros, M. McQuillan, D.J. Busch, A.S. Ibarraran-Viniegra, R. Sousa, E.M. Lafer, J.R. Morgan, Hsc70 ameliorates the vesicle recycling defects caused by excess alpha-synuclein at synapses, Eneuro 7 (2020) 0448-19.2020.
[35] J.K. Hannestad, S. Rocha, B. Agnarsson, V.P. Zhdanov, P. Wittung-Stafshede, F. Hook, Single-vesicle imaging reveals lipid-selective and stepwise membrane disruption by monomeric alpha-synuclein, Proceedings of the National Academy of Sciences of the United States of America 117 (2020) 14178-14186.
[36] A.H.V. Schapira, A.E.T. Lang, S. Fahn (Eds.), Movement Disorders 4: Blue Books of Neurology Series, Volume 35, Saunders, Philadelphia, PA, 2010.
[37] J.L. George, S. Mok, D. Moses, S. Wilkins, A.I. Bush, R.A. Cherny, D.I. Finkelstein, Targeting the progression of Parkinson's disease, Current Neuropharmacology 7 (2009) 9-36.
[38] A. Gupta, T.M. Dawson, Chapter 10 - pathogenesis of Parkinson's disease, Blue Books of Neurology 34 (2010) 155-169.
[39] S. Konzack, E. Thies, A. Marx, E.M. Mandelkow, E. Mandelkow, Swimming against the tide: Mobility of the microtubule-associated protein tau in neurons, Journal of Neuroscience 27 (2007) 9916-9927.
[40] S. Roy, M.J. Winton, M.M. Black, J.Q. Trojanowski, V.M.Y. Lee, Cytoskeletal requirements in axonal transport of slow component-b, Journal of Neuroscience 28 (2008) 5248-5256.

[41] A. Saha, J. Hill, M. Utton, A. Asuni, S. Ackerley, A. Grierson, C. Miller, A. Davies, V. Buchman, B. Anderton, D. Hanger, Parkinson's disease alpha-synuclein mutations exhibit defective axonal transport in cultured neurons, Journal of Cell Science 117 (2004) 1017-1024.
[42] I.A. Kuznetsov, A.V. Kuznetsov, Bidirectional, unlike unidirectional transport, allows transporting axonal cargos against their concentration gradient, bioRxiv (2021) doi: https://doi.org/10.1101/2021.01.27.428531.
[43] J. Burre, The synaptic function of alpha-synuclein, Journal of Parkinsons Disease 5 (2015) 699-713.
[44] D.L. Fortin, V.M. Nemani, K. Nakamura, R.H. Edwards, The behavior of alpha-synuclein in neurons, Movement Disorders 25 (2010) S21-S26.
[45] D. Snead, D. Eliezer, Alpha-synuclein function and dysfunction on cellular membranes, Experimental Neurobiology 23 (2014) 292-313.
[46] Z.L. Almeida, R.M.M. Brito, Structure and aggregation mechanisms in amyloids, Molecules 25 (2020) 1195.
[47] A.M. Morris, R.G. Finke, Alpha-synuclein aggregation variable temperature and variable pH kinetic data: A re-analysis using the finke-watzky 2-step model of nucleation and autocatalytic growth, Biophysical Chemistry 140 (2009) 9-15.
[48] A.K. Frimpong, R.R. Abzatimov, V.N. Uversky, I.A. Kaltashov, Characterization of intrinsically disordered proteins with electrospray ionization mass spectrometry: Conformational heterogeneity of alpha-synuclein, Proteins-Structure Function and Bioinformatics 78 (2010) 714-722.
[49] H.A. Lashuel, C.R. Overk, A. Oueslati, E. Masliah, The many faces of alpha-synuclein: From structure and toxicity to therapeutic target, Nature Reviews Neuroscience 14 (2013) 38-48.
[50] Z. Huang, H.G. Khaled, M. Kirschmann, S.M.H. Gobes, R.H.R. Hahnloser, Excitatory and inhibitory synapse reorganization immediately after critical sensory experience in a vocal learner, Elife 7 (2018) e37571.
[51] L. Siksou, P. Rostaing, J. Lechaire, T. Boudier, T. Ohtsuka, A. Fejtova, H. Kao, P. Greengard, E.D. Gundelfinger, A. Triller, S. Marty, Three-dimensional architecture of presynaptic terminal cytomatrix, Journal of Neuroscience 27 (2007) 6868-6877.
[52] J.P. Bolam, E.K. Pissadaki, Living on the edge with too many mouths to feed: Why dopamine neurons die, Movement Disorders 27 (2012) 1478-1483.
[53] D. Haddad, K. Nakamura, Understanding the susceptibility of dopamine neurons to mitochondrial stressors in Parkinson's disease, FEBS Letters 589 (2015) 3702-3713.
[54] H. Lee, C. Choi, S. Lee, Membrane-bound alpha-synuclein has a high aggregation propensity and the ability to seed the aggregation of the cytosolic form, Journal of Biological Chemistry 277 (2002) 671-678.

[55] F. Miraglia, A. Ricci, L. Rota, E. Colla, Subcellular localization of alpha-synuclein aggregates and their interaction with membranes, Neural Regeneration Research 13 (2018) 1136-1144.
[56] B. Dehay, J. Bove, N. Rodriguez-Muela, C. Perier, A. Recasens, P. Boya, M. Vila, Pathogenic lysosomal depletion in Parkinson's disease, Journal of Neuroscience 30 (2010) 12535-12544.
[57] M.P. Jackson, E.W. Hewitt, Cellular proteostasis: Degradation of misfolded proteins by lysosomes, Proteostasis 60 (2016) 173-180.
[58] A. Brown, Axonal transport of membranous and nonmembranous cargoes: A unified perspective, Journal of Cell Biology 160 (2003) 817-821.
[59] D. Li, J. Shi, C. Mao, S. Liu, J. Wang, J. Chen, F. Wang, Y. Yang, W. Hu, L. Hu, C. Liu, Alteration of dynein function affects alpha-synuclein degradation via the autophagosome-lysosome pathway, International Journal of Molecular Sciences 14 (2013) 24242-24254.
[60] L.A. Volpicelli-Daley, Effects of alpha-synuclein on axonal transport, Neurobiology of Disease 105 (2017) 321-327.
[61] L. Wang, U. Das, D.A. Scott, Y. Tang, P.J. McLean, S. Roy, Alpha-synuclein multimers cluster synaptic vesicles and attenuate recycling, Current Biology 24 (2014) 2319-2326.
[62] T. Bartels, A traffic jam leads to Lewy bodies, Nature Neuroscience 22 (2019) 1043-1045.
[63] S. Gribaudo, P. Tixador, L. Bousset, A. Fenyi, P. Lino, R. Melki, J. Peyrin, A.L. Perrier, Propagation of alpha-synuclein strains within human reconstructed neuronal network, Stem Cell Reports 12 (2019) 230-244.
[64] D.A. Smith, R.M. Simmons, Models of motor-assisted transport of intracellular particles, Biophysical Journal 80 (2001) 45-68.
[65] A. Mahul-Mellier, J. Burtscher, N. Maharjan, L. Weerens, M. Croisier, F. Kuttler, M. Leleu, G.W. Knott, H.A. Lashuel, The process of Lewy body formation, rather than simply alpha-synuclein fibrillization, is one of the major drivers of neurodegeneration, Proceedings of the National Academy of Sciences of the United States of America 117 (2020) 4971-4982.
[66] E. Kuusisto, L. Parkkinen, I. Alafuzoff, Morphogenesis of Lewy bodies: Dissimilar incorporation of alpha-synuclein, ubiquitin, and p62, Journal of Neuropathology and Experimental Neurology 62 (2003) 1241-1253.
[67] E. Hellstrand, A. Nowacka, D. Topgaard, S. Linse, E. Sparr, Membrane lipid co-aggregation with alpha-synuclein fibrils, Plos One 8 (2013) e77235.
[68] T. Nakata, S. Terada, N. Hirokawa, Visualization of the dynamics of synaptic vesicle and plasma membrane proteins in living axons, Journal of Cell Biology 140 (1998) 659-674.

[69] E. Moubarak, D. Engel, M.A. Dufour, M. Tapia, F. Tell, J. Goaillard, Robustness to axon initial segment variation is explained by somatodendritic excitability in rat substantia nigra dopaminergic neurons, Journal of Neuroscience 39 (2019) 5044-5063.
[70] R. Wang, J. Zhao, J. Zhang, W. Liu, M. Zhao, J. Li, J. Lv, Y. Li, Effect of lysosomal and ubiquitin-proteasome system dysfunction on the abnormal aggregation of alpha-synuclein in PC12 cells, Experimental and Therapeutic Medicine 9 (2015) 2088-2094.
[71] L. Rodriguez, M.M. Marano, A. Tandon, Import and export of misfoldeda alpha-synuclein, Frontiers in Neuroscience 12 (2018) 344.
[72] E. Pannese, Neurocytology: Fine Structure of Neurons, Nerve Processes, and Neuroglial Cells, 2nd, Springer, New York, 2015.
[73] D. Fortin, V. Nemani, S. Voglmaier, M. Anthony, T. Ryan, R. Edwards, Neural activity controls the synaptic accumulation of alpha-synuclein, Journal of Neuroscience 25 (2005) 10913-10921.
[74] M. Bourdenx, E. Bezard, B. Dehay, Lysosomes and alpha-synuclein form a dangerous duet leading to neuronal cell death, Frontiers in Neuroanatomy 8 (2014) 83.
[75] G. Bellomo, S. Paciotti, L. Gatticchi, L. Parnetti, The vicious cycle between alpha-synuclein aggregation and autophagic-lysosomal dysfunction, Movement Disorders 35 (2020) 34-44.
[76] W. Poewe, K. Seppi, C.M. Tanner, G.M. Halliday, P. Brundin, J. Volkmann, A. Schrag, A.E. Lang, Parkinson disease, Nature Reviews Disease Primers 3 (2017) UNSP 17013.
[77] A. Hoffmann, G. Minakaki, S. Menges, R. Salvi, S. Savitskiy, A. Kazman, H. Vicente Miranda, D. Mielenz, J. Klucken, J. Winkler, W. Xiang, Extracellular aggregated alpha synuclein primarily triggers lysosomal dysfunction in neural cells prevented by trehalose, Scientific Reports 9 (2019) 544.
[78] C.R. Fields, N. Bengoa-Vergniory, R. Wade-Martins, Targeting alpha-synuclein as a therapy for Parkinson's disease, Frontiers in Molecular Neuroscience 12 (2019) 299.
[79] J. Wagner, S. Ryazanov, A. Leonov, J. Levin, S. Shi, F. Schmidt, C. Prix, F. Pan-Montojo, U. Bertsch, G. Mitteregger-Kretzschmar, M. Geissen, M. Eiden, F. Leidel, T. Hirschberger, A.A. Deeg, J.J. Krauth, W. Zinth, P. Tavan, J. Pilger, M. Zweckstetter, T. Frank, M. Baehr, J.H. Weishaupt, M. Uhr, H. Urlaub, U. Teichmann, M. Samwer, K. Boetzel, M. Groschup, H. Kretzschmar, C. Griesinger, A. Giese, Anle138b: A novel oligomer modulator for disease-modifying therapy of neurodegenerative diseases such as prion and Parkinson's disease, Acta Neuropathologica 125 (2013) 795-813.
[80] D. Mehta, R. Jackson, G. Paul, J. Shi, M. Sabbagh, Why do trials for Alzheimer's disease drugs keep failing? A discontinued drug perspective for 2010-2015, Expert Opinion on Investigational Drugs 26 (2017) 735-739.

[81] D.J. Selkoe, J. Hardy, The amyloid hypothesis of Alzheimer's disease at 25years, Embo Molecular Medicine 8 (2016) 595-608.
[82] J.V. Beck, K.J. Arnold, Parameter Estimation in Science and Engineering, Wiley, New York, 1977.
[83] K.S. Zadeh, H.J. Montas, A class of exact solutions for biomacromolecule diffusion-reaction in live cells, Journal of Theoretical Biology 264 (2010) 914-933.
[84] Z. Zi, Sensitivity analysis approaches applied to systems biology models, Iet Systems Biology 5 (2011) 336-346.
[85] I.A. Kuznetsov, A.V. Kuznetsov, Investigating sensitivity coefficients characterizing the response of a model of tau protein transport in an axon to model parameters, Computer Methods in Biomechanics and Biomedical Engineering 22 (2019) 71-83.
[86] H. Kacser, J. Burns, D. Fell, The control of flux, Biochemical Society Transactions 23 (1995) 341-366.
[87] B.A. Killinger, R. Melki, P. Brundin, J.H. Kordower, Endogenous alpha-synuclein monomers, oligomers and resulting pathology: Let's talk about the lipids in the room, Npj Parkinsons Disease 5 (2019) 23.
[88] D. Boassa, M.L. Berlanga, M.A. Yang, M. Terada, J. Hu, E.A. Bushong, M. Hwang, E. Masliah, J.M. George, M.H. Ellisman, Mapping the subcellular distribution of alpha-synuclein in neurons using genetically encoded probes for correlated light and electron microscopy: Implications for Parkinson's disease pathogenesis, Journal of Neuroscience 33 (2013) 2605-2615.
[89] F. Miraglia, V. Valvano, L. Rota, C. Di Primio, V. Quercioli, L. Betti, G. Giannaccini, A. Cattaneo, E. Colla, Alpha-synuclein FRET biosensors reveal early alpha-synuclein aggregation in the endoplasmic reticulum, Life-Basel 10 (2020) 147.
[90] N. Giguere, S.B. Nanni, L. Trudeau, On cell loss and selective vulnerability of neuronal populations in Parkinson's disease, Frontiers in Neurology 9 (2018) 455.
[91] D.A. Scott, I. Tabarean, Y. Tang, A. Cartier, E. Masliah, S. Roy, A pathologic cascade leading to synaptic dysfunction in alpha-synuclein-induced neurodegeneration, Journal of Neuroscience 30 (2010) 8083-8095.
[92] K.J. Spinelli, J.K. Taylor, V.R. Osterberg, M.J. Churchill, E. Pollock, C. Moore, C.K. Meshul, V.K. Unni, Presynaptic alpha-synuclein aggregation in a mouse model of Parkinson's disease, Journal of Neuroscience 34 (2014) 2037-2050.
[93] S. Fanning, D. Selkoe, U. Dettmer, Vesicle trafficking and lipid metabolism in synucleinopathy, Acta Neuropathologica 141 (2021) 491-510.

[94] Figure Generated with the Aid of Servier Medical Art, Licensed Under a Creative Common Attribution 3.0 Generic License. http://smart.servier.com.

Figure captions

Fig. 1. A diagram of a neuron showing transport of α-syn monomers and misfolded aggregates in the axon and catalytic effect of α-syn aggregates leading to the formation of aggregates of membrane-bound organelles (which later become LBs and LNs). Demand sites are numbered starting with the most proximal (#1) to the most distal (#*N*) [94].

Fig. 2. Kinetic diagrams showing various kinetic states in the following sub-models:

(a) in the sub-model of slow axonal transport of α-syn monomers from the soma to the synapse. The diagram is based on the model of SCa transport of neurofilaments [25], which was modified in [26,27] to extend it to SCb transport of cytosolic proteins.

(b) in the sub-model simulating transitions between various states of α-syn in the presynaptic terminal: α-syn monomers suspended in the cytosol, α-syn monomers bound to the membrane, and α-syn aggregated in the cytosol;

(c) in the sub-model of fast axonal transport of α-syn aggregates from the presynaptic terminal to the soma;

(d) in the sub-model of fast axonal transport of various vesicles from the soma to the presynaptic terminal and their aggregation that is presumably catalyzed by α-syn aggregates;

(e) in the sub-model simulating vesicle aggregation in the soma, which is presumably catalyzed by α-syn aggregates, and also simulating the destruction of α-syn aggregates in the somatic lysosomes.

Fig. 3. (a) Various linear concentrations (per unit length of the axon) of α-syn monomers in the axon, including the total concentration, which is the sum of α-syn concentrations in motor-driven, pausing, and diffusing states. (b) Total flux of α-syn monomers due to active transport, powered by molecular motors, and diffusion in the cytosol. $T^*_{B,1/2,s} = 2.59 \times 10^5$ s. $k^*_{10} = 3 \times 10^{-7}$ s^{-1}.

Fig. 4. (a) Volumetric concentrations of α-syn monomers and α-syn aggregates in the presynaptic terminal and surface concentration of α-syn monomers bound to the presynaptic membrane. (b) Volumetric concentration of α-syn aggregates in the presynaptic terminal (same as in (a), but on the enlarged scale). $T^*_{B,1/2,s} = 2.59 \times 10^5$ s. $k^*_{10} = 3 \times 10^{-7}$ s^{-1}.

Fig. 5. Linear concentrations (per unit length of the axon) of retrogradely transported α-syn aggregates and free α-syn aggregates in the axon. $T^*_{B,1/2,s} = 2.59\times10^5$ s. $k^*_{10} = 3\times10^{-7}$ s^{-1}.

Fig. 6. Total area of membrane in all membrane-bound organelles that are actively anterogradely transported in the axon and in all membrane-bound organelles that are detached from MTs, per unit length of the axon. Also, the anterograde flux of membrane due to transport of membrane-bound organelles. $T^*_{B,1/2,s} = 2.59\times10^5$ s. $k^*_{10} = 3\times10^{-7}$ s^{-1}.

Fig. 7. (a) Total area of the membrane in all vesicle aggregates in the axon, per unit length of the axon, vs x^*, at t^*=3.17 years. (b) Total area of the membrane in all vesicle aggregates in the axon, per unit length of the axon, vs time, at $x^*=L^*/2$. $T^*_{B,1/2,s} = 2.59\times10^5$ s. $k^*_{10} = 3\times10^{-7}$ s^{-1}.

Fig. 8. (a) Volumetric concentration of α-syn aggregates in the cytosol of the soma. (b) Volumetric concentration of membrane surrounding membrane-bound vesicles in the soma, and membrane contained in fragments and fragmented organelles in the soma. $T^*_{B,1/2,s} = 2.59\times10^5$ s and $T^*_{B,1/2,s} = 2.59\times10^{10}$ s. $k^*_{10} = 3\times10^{-7}$ s^{-1}. The curves marked by "no α-syn 1 year" are computed under the assumption that all α-syn aggregates are removed (by enhancing their destruction via autophagosomes) 1 year after the beginning of the α-syn aggregation process.

Fig. 9. (a) Volumetric concentration of α-syn aggregates in the cytosol of the soma. (b) Volumetric concentration of membrane surrounding membrane-bound vesicles in the soma, and membrane contained in fragments and fragmented organelles in the soma. $T^*_{B,1/2,s} = 2.59\times10^5$ s and $T^*_{B,1/2,s} = 2.59\times10^{10}$ s. $k^*_{10} = 3\times10^{-10}$ s^{-1}.

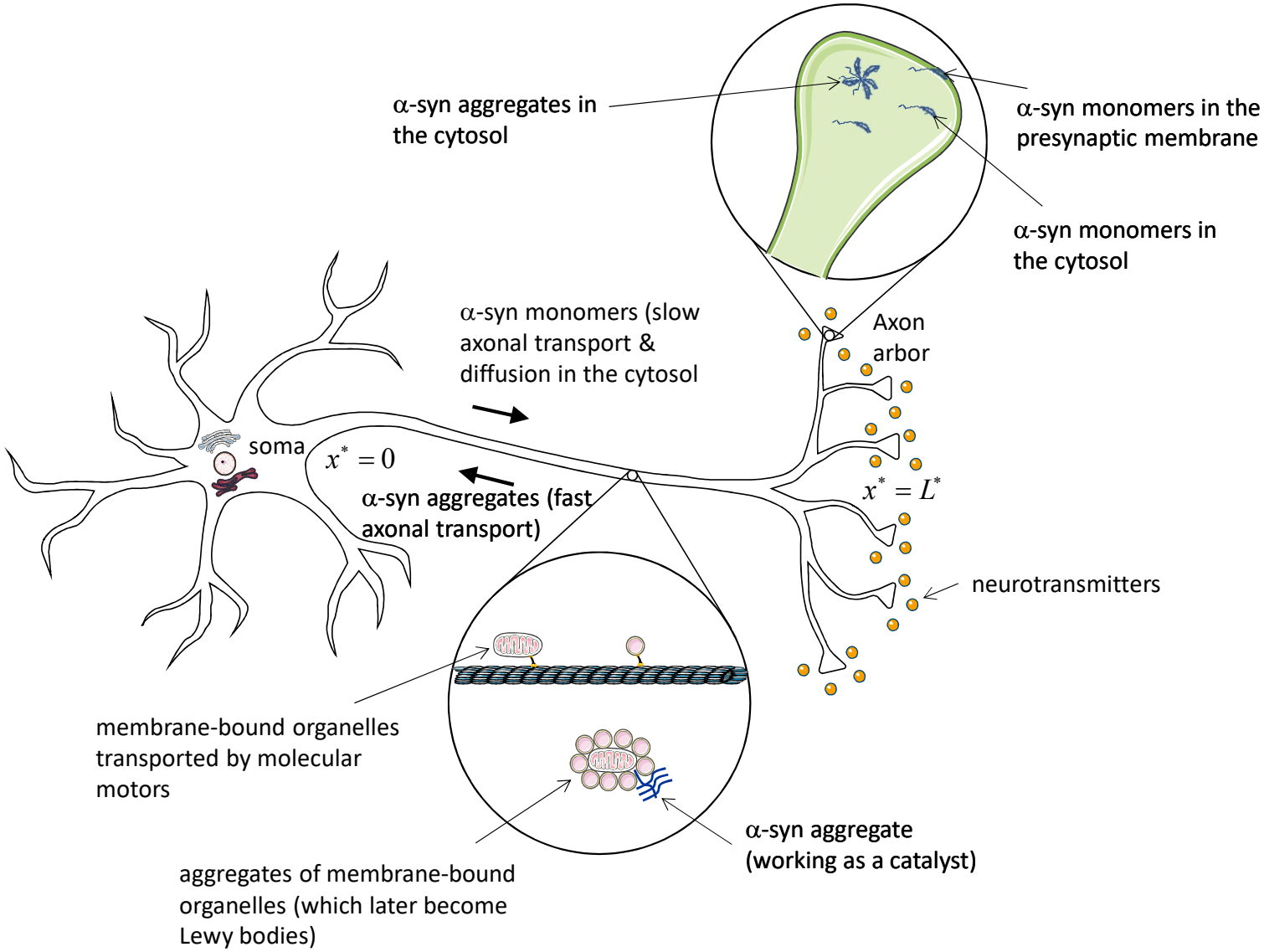
α-syn aggregates in the cytosol
α-syn monomers in the presynaptic membrane
α-syn monomers in the cytosol
α-syn monomers (slow axonal transport & diffusion in the cytosol
Axon arbor
soma
$x^* = 0$
α-syn aggregates (fast axonal transport)
$x^* = L^*$
neurotransmitters
membrane-bound organelles transported by molecular motors
α-syn aggregate (working as a catalyst)
aggregates of membrane-bound organelles (which later become Lewy bodies)

Figure 1

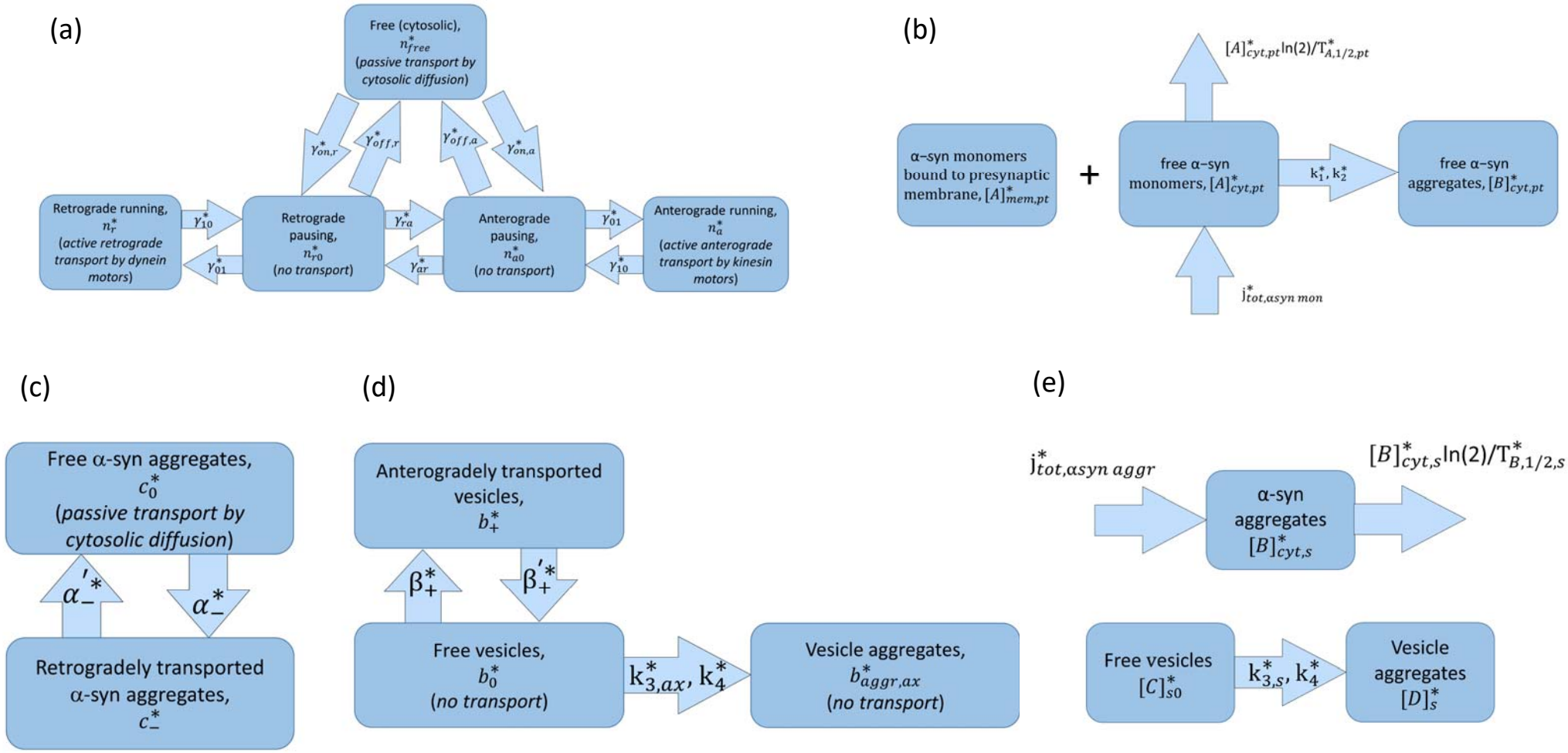
(a)
Free (cytosolic), n^*_{free} (passive transport by cytosolic diffusion)
$\gamma^*_{on,r}$
$\gamma^*_{off,r}$
$\gamma^*_{off,a}$
$\gamma^*_{on,a}$
Retrograde running, n^*_r (active retrograde transport by dynein motors)
γ^*_{10}
γ^*_{01}
Retrograde pausing, n^*_{r0} (no transport)
γ^*_{ra}
γ^*_{ar}
Anterograde pausing, n^*_{a0} (no transport)
γ^*_{01}
γ^*_{10}
Anterograde running, n^*_a (active anterograde transport by kinesin motors)
(b)
$[A]^*_{cyt,pt}\ln(2)/T^*_{A,1/2,pt}$
α–syn monomers bound to presynaptic membrane, $[A]^*_{mem,pt}$
+
free α–syn monomers, $[A]^*_{cyt,pt}$
k^*_1, k^*_2
free α–syn aggregates, $[B]^*_{cyt,pt}$
$j^*_{tot,\alpha syn\ mon}$
(c)
Free α-syn aggregates, c^*_0 (passive transport by cytosolic diffusion)
α'^*_-
α^*_-
Retrogradely transported α-syn aggregates, c^*_-
(d)
Anterogradely transported vesicles, b^*_+
β^*_+
β'^*_+
Free vesicles, b^*_0 (no transport)
$k^*_{3,ax}, k^*_4$
Vesicle aggregates, $b^*_{aggr,ax}$ (no transport)
(e)
$j^*_{tot,\alpha syn\ aggr}$
α-syn aggregates $[B]^*_{cyt,s}$
$[B]^*_{cyt,s}\ln(2)/T^*_{B,1/2,s}$
Free vesicles $[C]^*_{s0}$
$k^*_{3,s}, k^*_4$
Vesicle aggregates $[D]^*_s$

Figure 2

(a)

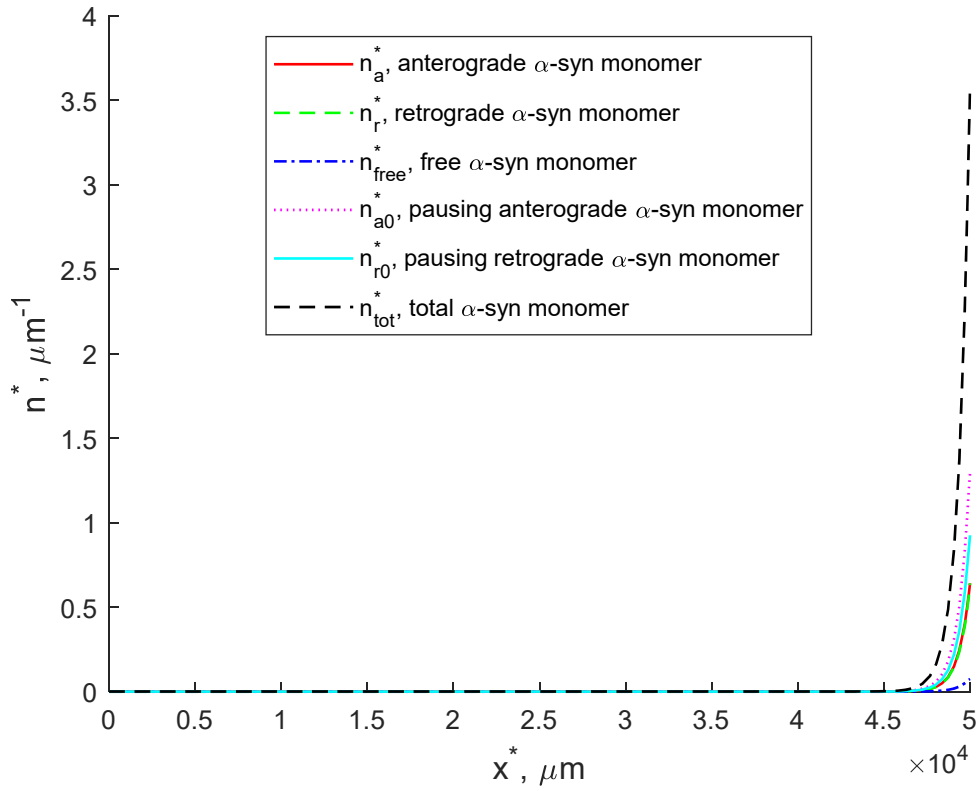
n^*_a, anterograde α-syn monomer
n^*_r, retrograde α-syn monomer
n^*_{free}, free α-syn monomer
n^*_{a0}, pausing anterograde α-syn monomer
n^*_{r0}, pausing retrograde α-syn monomer
n^*_{tot}, total α-syn monomer
n^*, μm^{-1}
x^*, μm
$\times 10^4$

(b)

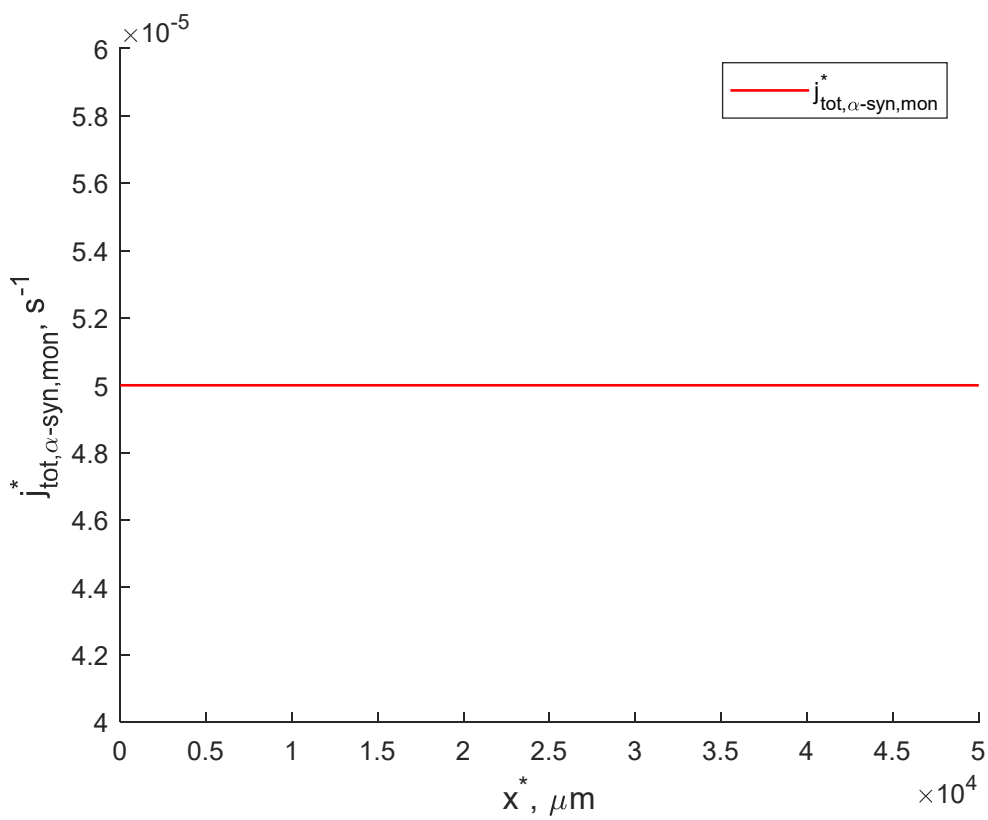
$\times 10^{-5}$
$j^*_{tot,\alpha\text{-syn,mon}}$
$j^*_{tot,\alpha\text{-syn,mon}}$, s^{-1}
x^*, μm
$\times 10^4$

Figure 3

(a)

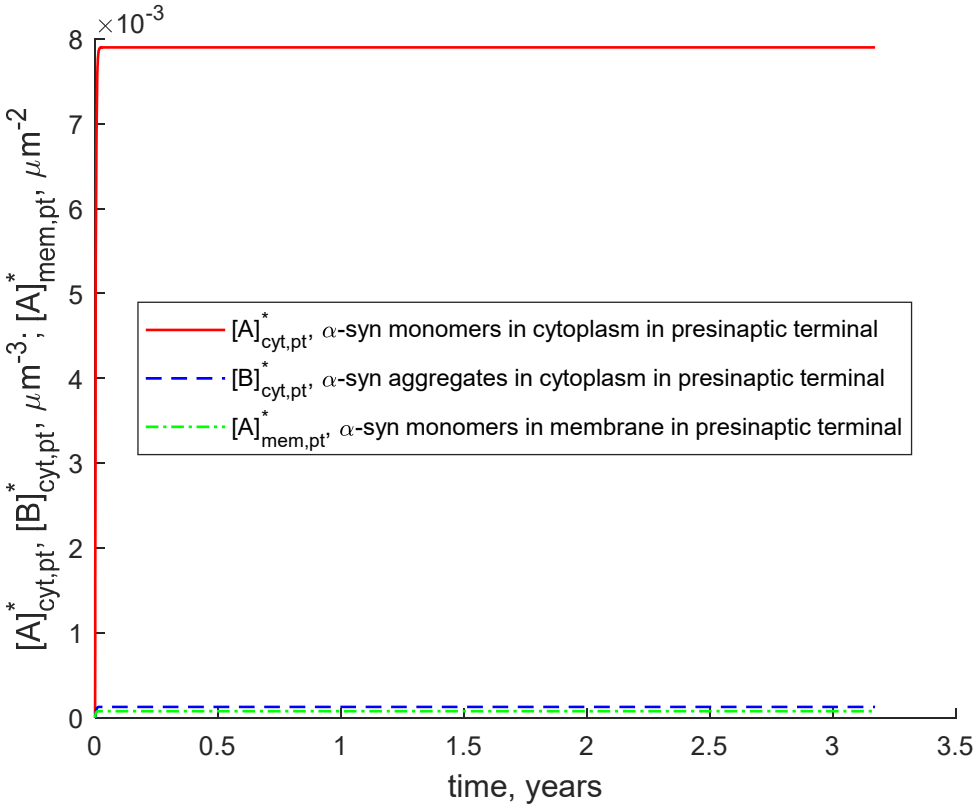
×10^-3
8
7
6
5
4
3
2
1
0
0
0.5
1
1.5
2
2.5
3
3.5
time, years
[A]*cyt,pt, [B]*cyt,pt, μm^-3; [A]*mem,pt, μm^-2
[A]*cyt,pt, α-syn monomers in cytoplasm in presinaptic terminal
[B]*cyt,pt, α-syn aggregates in cytoplasm in presinaptic terminal
[A]*mem,pt, α-syn monomers in membrane in presinaptic terminal

(b)

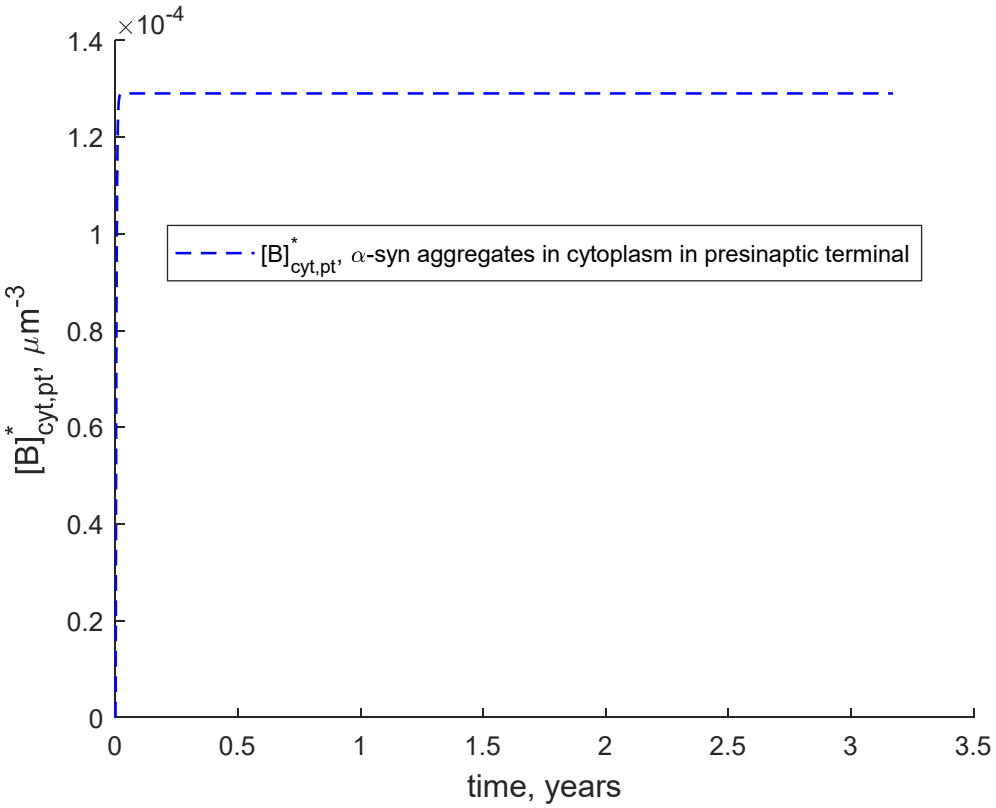
×10^-4
1.4
1.2
1
0.8
0.6
0.4
0.2
0
0
0.5
1
1.5
2
2.5
3
3.5
time, years
[B]*cyt,pt, μm^-3
[B]*cyt,pt, α-syn aggregates in cytoplasm in presinaptic terminal

Figure 4

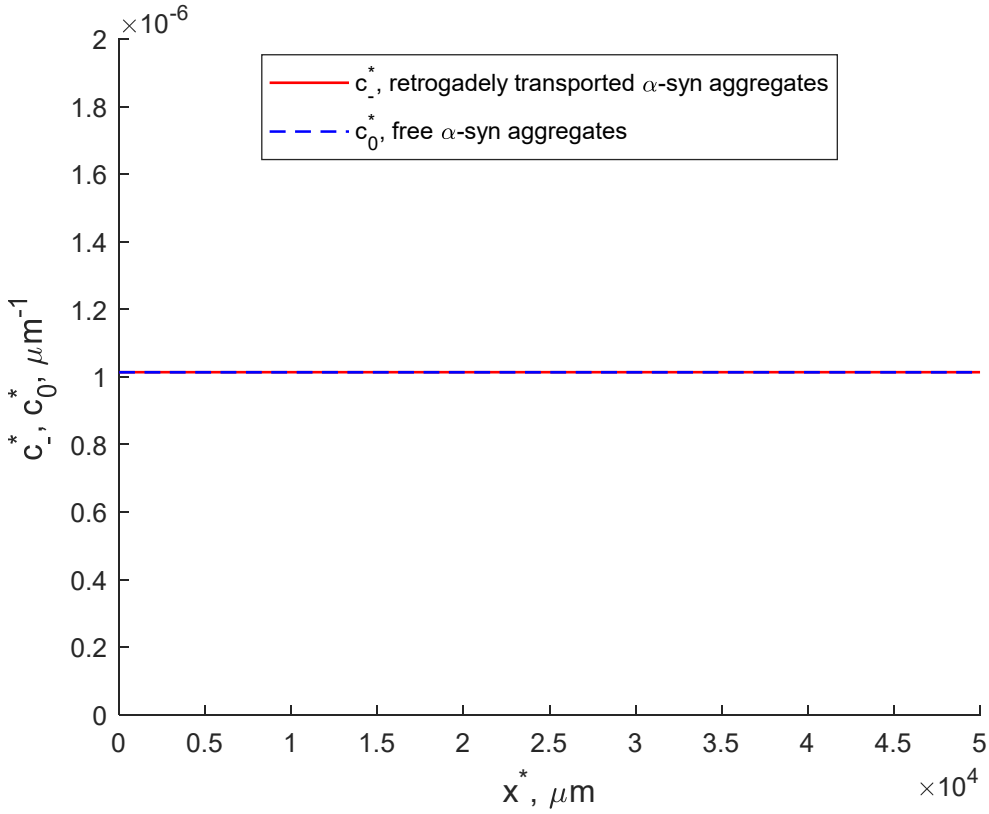
×10^-6
2
1.8
1.6
1.4
1.2
1
0.8
0.6
0.4
0.2
0
c*-, c*0, μm^-1
c*-, retrogadely transported α-syn aggregates
c*0, free α-syn aggregates
0
0.5
1
1.5
2
2.5
3
3.5
4
4.5
5
x*, μm
×10^4

Figure 5

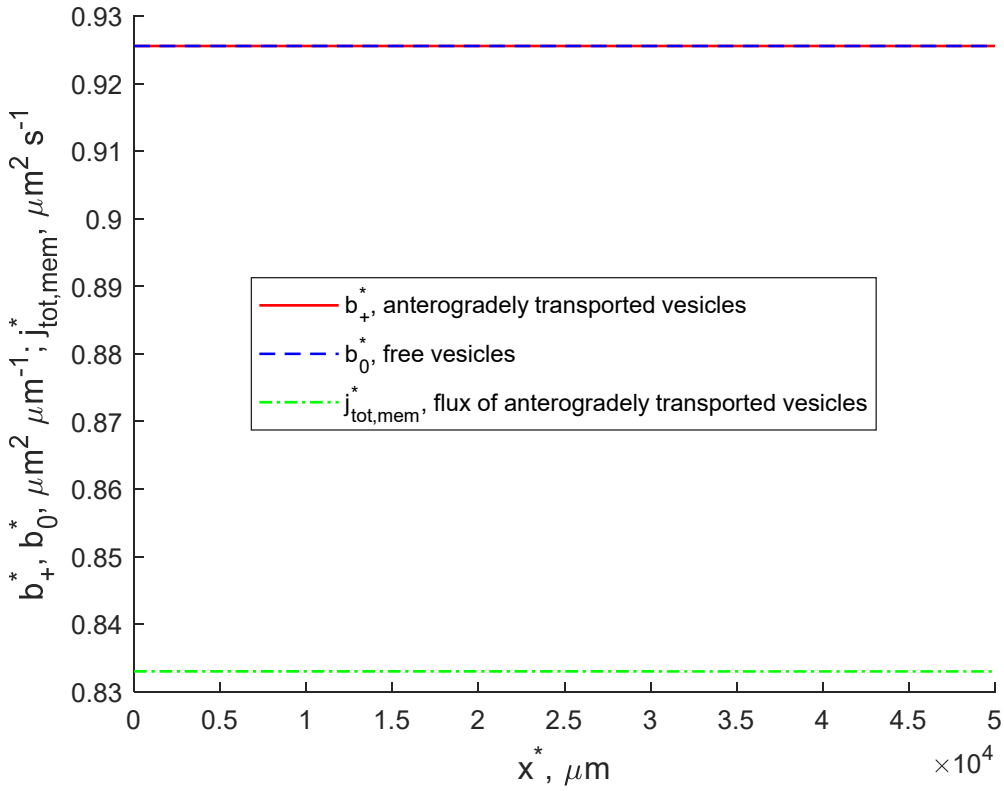
0.93
0.92
0.91
0.9
0.89
0.88
0.87
0.86
0.85
0.84
0.83
0
0.5
1
1.5
2
2.5
3
3.5
4
4.5
5
×10^4
x*, μm
b*+, b*0, μm^2 μm^-1; j*tot,mem, μm^2 s^-1
b*+, anterogradely transported vesicles
b*0, free vesicles
j*tot,mem, flux of anterogradely transported vesicles

Figure 6

(a)

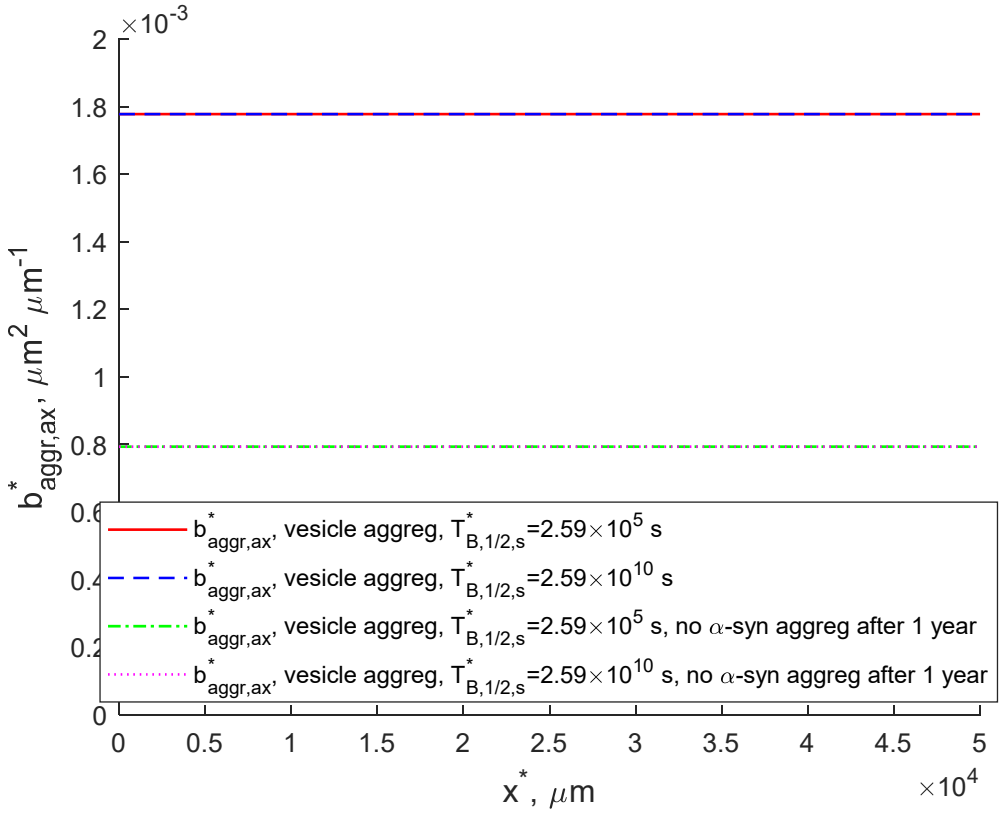
×10^-3
2
1.8
1.6
1.4
1.2
1
0.8
0.6
0.4
0.2
0
b*aggr,ax, μm^2 μm^-1
b*aggr,ax, vesicle aggreg, T*B,1/2,s=2.59×10^5 s
b*aggr,ax, vesicle aggreg, T*B,1/2,s=2.59×10^10 s
b*aggr,ax, vesicle aggreg, T*B,1/2,s=2.59×10^5 s, no α-syn aggreg after 1 year
b*aggr,ax, vesicle aggreg, T*B,1/2,s=2.59×10^10 s, no α-syn aggreg after 1 year
0
0.5
1
1.5
2
2.5
3
3.5
4
4.5
5
x*, μm
×10^4

(b)

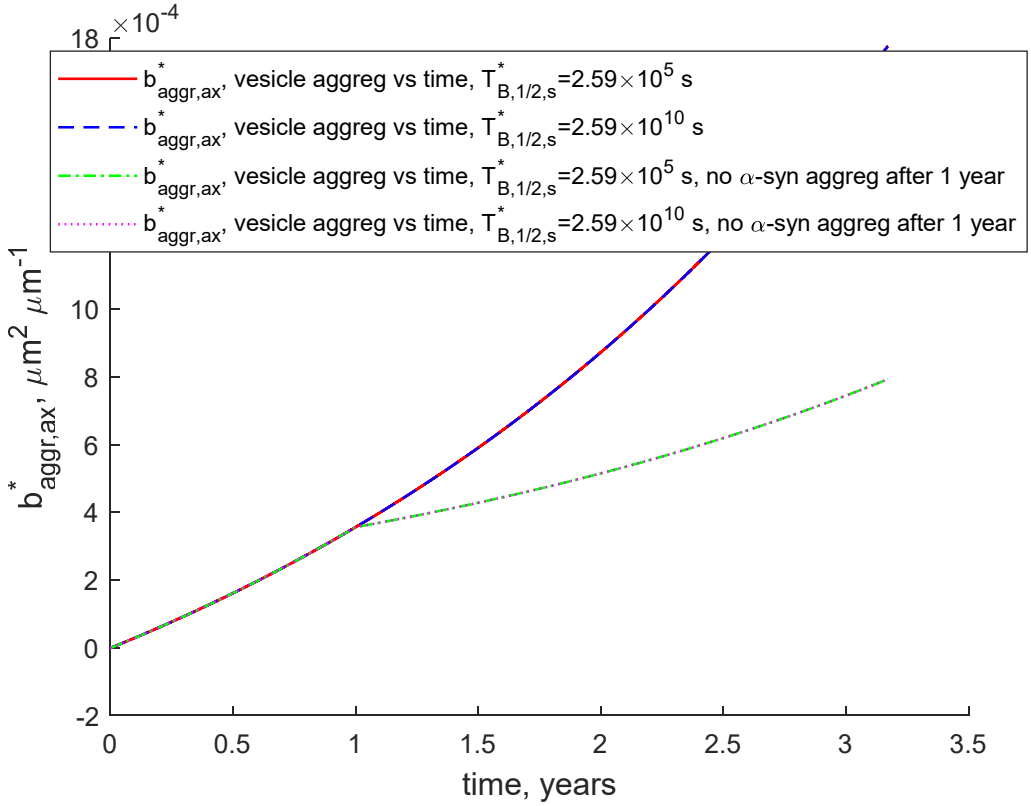
×10^-4
18
10
8
6
4
2
0
-2
b*aggr,ax, μm^2 μm^-1
b*aggr,ax, vesicle aggreg vs time, T*B,1/2,s=2.59×10^5 s
b*aggr,ax, vesicle aggreg vs time, T*B,1/2,s=2.59×10^10 s
b*aggr,ax, vesicle aggreg vs time, T*B,1/2,s=2.59×10^5 s, no α-syn aggreg after 1 year
b*aggr,ax, vesicle aggreg vs time, T*B,1/2,s=2.59×10^10 s, no α-syn aggreg after 1 year
0
0.5
1
1.5
2
2.5
3
3.5
time, years

Figure 7

(a)

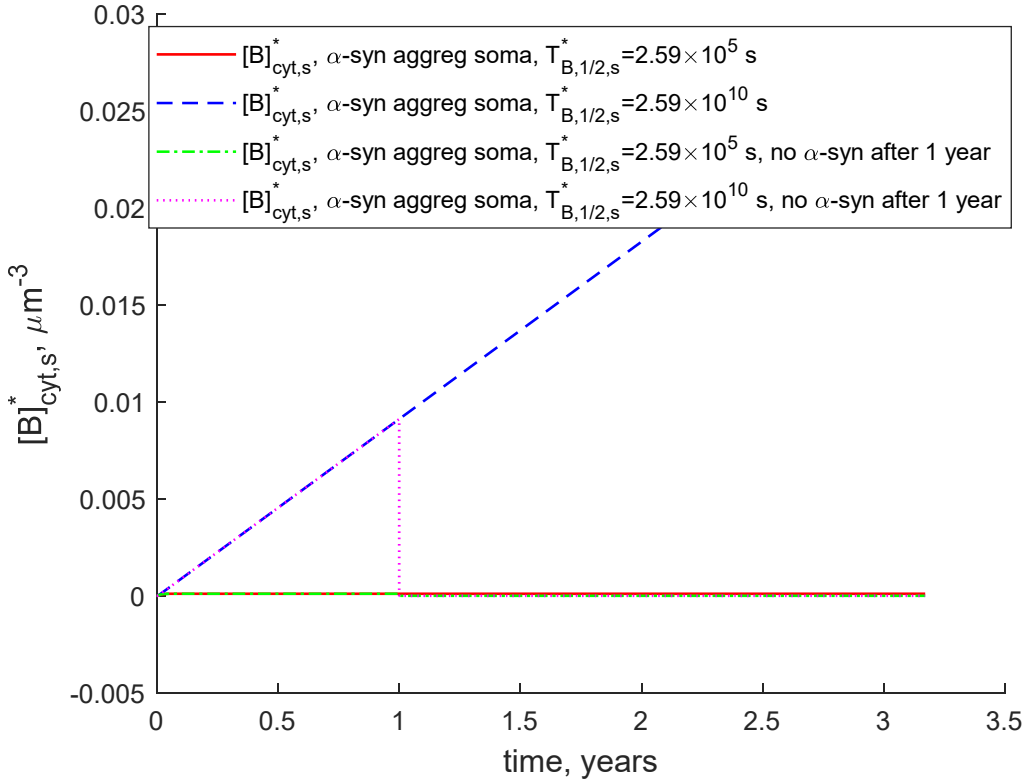
[B]*cyt,s, α-syn aggreg soma, T*B,1/2,s=2.59×10^5 s
[B]*cyt,s, α-syn aggreg soma, T*B,1/2,s=2.59×10^10 s
[B]*cyt,s, α-syn aggreg soma, T*B,1/2,s=2.59×10^5 s, no α-syn after 1 year
[B]*cyt,s, α-syn aggreg soma, T*B,1/2,s=2.59×10^10 s, no α-syn after 1 year
[B]*cyt,s, μm^-3
time, years
0.03
0.025
0.02
0.015
0.01
0.005
0
-0.005
0
0.5
1
1.5
2
2.5
3
3.5

(b)

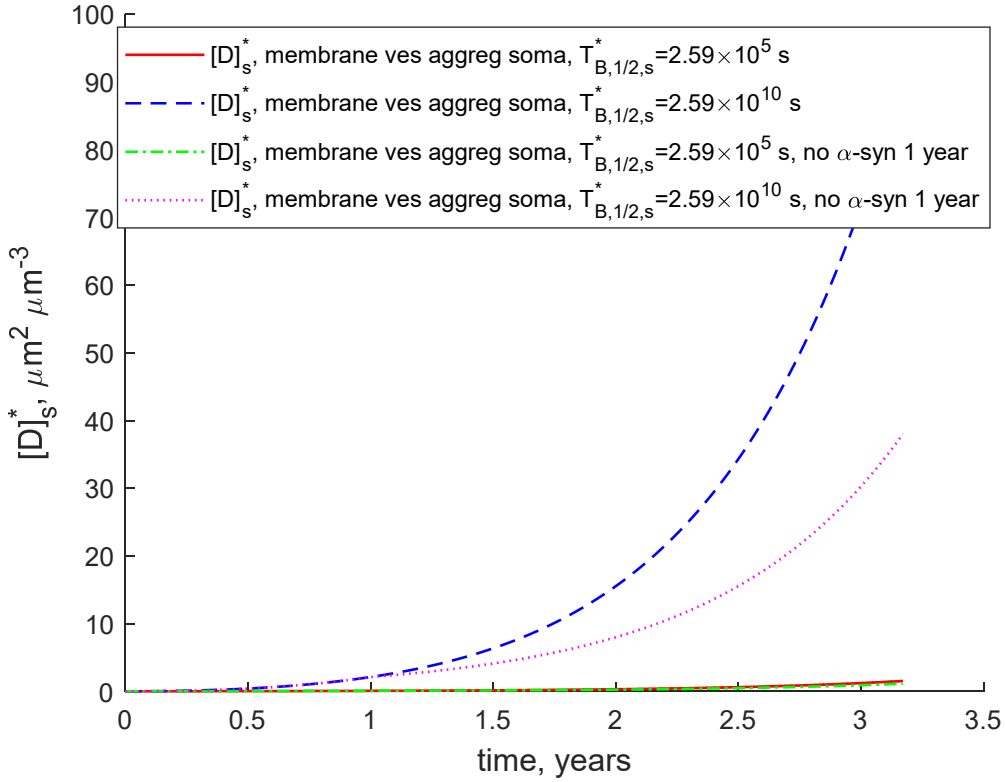
[D]*s, membrane ves aggreg soma, T*B,1/2,s=2.59×10^5 s
[D]*s, membrane ves aggreg soma, T*B,1/2,s=2.59×10^10 s
[D]*s, membrane ves aggreg soma, T*B,1/2,s=2.59×10^5 s, no α-syn 1 year
[D]*s, membrane ves aggreg soma, T*B,1/2,s=2.59×10^10 s, no α-syn 1 year
[D]*s, μm^2 μm^-3
time, years
100
90
80
70
60
50
40
30
20
10
0
0
0.5
1
1.5
2
2.5
3
3.5

Figure 8

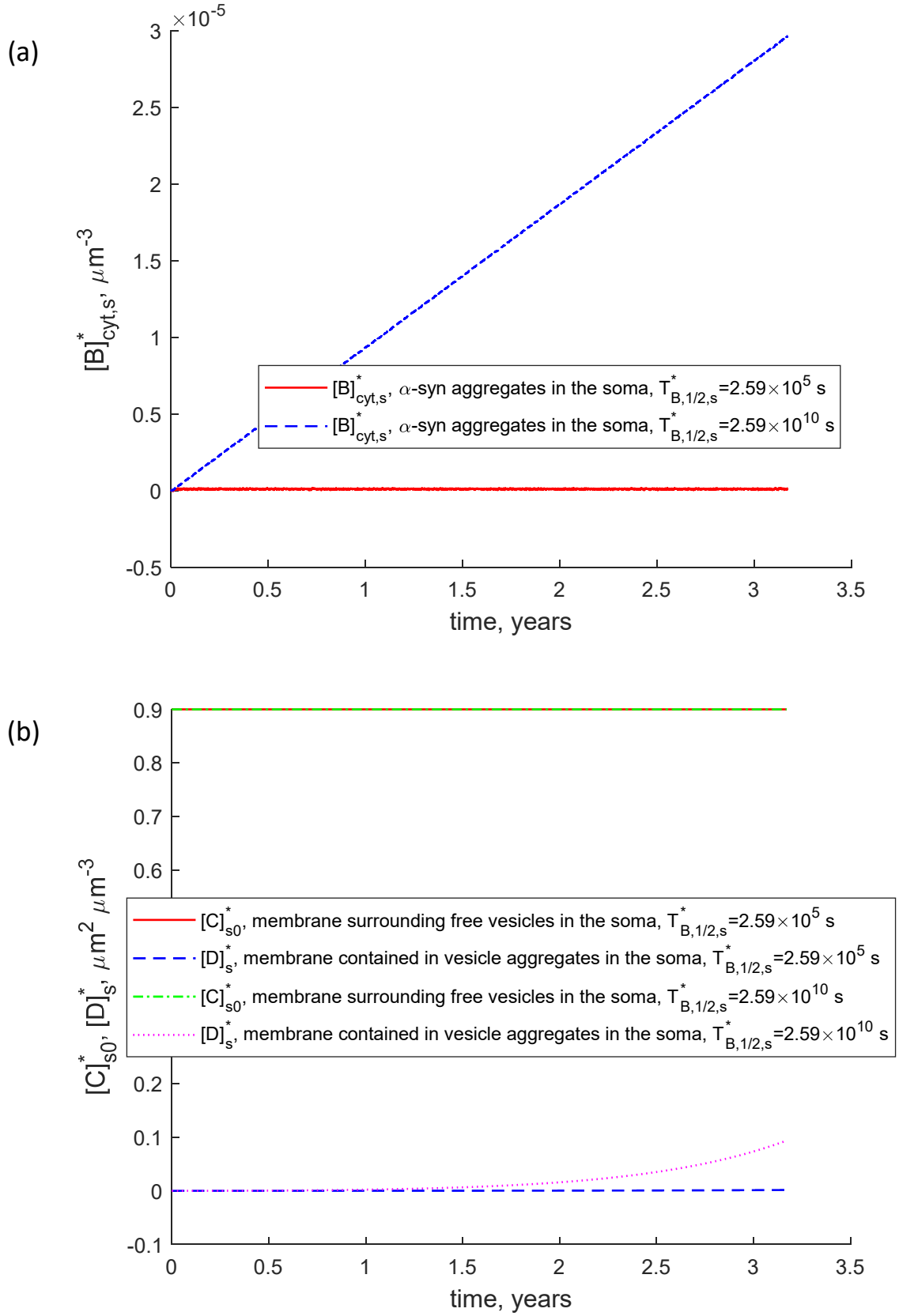
(a)
×10^-5
3
2.5
2
1.5
1
0.5
0
-0.5
[B]*cyt,s, μm^-3
[B]*cyt,s, α-syn aggregates in the soma, T*B,1/2,s=2.59×10^5 s
[B]*cyt,s, α-syn aggregates in the soma, T*B,1/2,s=2.59×10^10 s
0
0.5
1
1.5
2
2.5
3
3.5
time, years
(b)
0.9
0.8
0.7
0.6
0.2
0.1
0
-0.1
[C]*s0, [D]*s, μm^2 μm^-3
[C]*s0, membrane surrounding free vesicles in the soma, T*B,1/2,s=2.59×10^5 s
[D]*s, membrane contained in vesicle aggregates in the soma, T*B,1/2,s=2.59×10^5 s
[C]*s0, membrane surrounding free vesicles in the soma, T*B,1/2,s=2.59×10^10 s
[D]*s, membrane contained in vesicle aggregates in the soma, T*B,1/2,s=2.59×10^10 s
0
0.5
1
1.5
2
2.5
3
3.5
time, years

Figure 9

Can the lack of fibrillar form of alpha-synuclein in Lewy bodies be explained by its catalytic activity?

I. A. Kuznetsov[(a), (b)] and A. V. Kuznetsov[(c)]

[(a)]Perelman School of Medicine, University of Pennsylvania, Philadelphia, PA 19104, USA

[(b)]Department of Bioengineering, University of Pennsylvania, Philadelphia, PA 19104, USA

[(c)]Dept. of Mechanical and Aerospace Engineering, North Carolina State University, Raleigh, NC 27695-7910, USA; e-mail: avkuznet@ncsu.edu

Supplemental Materials

S1. Tables

Table S1. Relative sensitivity of the total area of membrane in all vesicle aggregates in the axon (that later become LNs), $b^*_{aggr,ax}$, to parameters given in Table 9. Computations were performed using Eqs. (36) and (37) with (for example) $\Delta j^*_{tot,mem,x=0} = 10^{-3}\, j^*_{tot,mem,x=0}$.

$S^{b^*_{aggr,ax}}_{j^*_{tot,mem,x=0}}$	$S^{b^*_{aggr,ax}}_{v^*_+}$	$S^{b^*_{aggr,ax}}_{\beta^*_+}$	$S^{b^*_{aggr,ax}}_{\beta'^*_+}$	$S^{b^*_{aggr,ax}}_{k^*_{30,ax}}$	$S^{b^*_{aggr,ax}}_{k^*_{4,ax}}$
1.70	−1.69	−1.69	1.70	1.00	0.696